# Uncertainty-Aware ML Surrogates for DFT Strain–Bandgap Engineering in $CsSnX_3$ (X = Cl, Br, I)

Md. Nurul Amin[1*], Muhammad Mudassir Ahmad Alwi[2*], Muhammad Jawad[3], Monaf Hodhod[4]

[1]Jamal Nazrul Islam Research Centre for Mathematical and Physical Sciences, University of Chittagong, Chattogram, 4331, Bangladesh.
[2]Department of Materials Engineering, King Faisal University, Al Ahsa, Saudi Arabia.
[3]Faculty of Science Education, Jeju National University, Jeju 63243, Republic of Korea.
[4]Department of Mechanical Engineering, King Faisal University, Al Ahsa, Saudi Arabia.

*Corresponding author: nurulaminarju@gmail.com- Md. Nurul Amin, malwi@kfu.edu.sa-Muhammad Mudassir Ahmad Alwi

Table S1: Model benchmarking by material and loading mode. For each curve we list the algorithm, training size $N_{\text{train}}$, and leave-one-out cross-validation metrics (RMSE, MAE, $R^2$). Lower is better for RMSE/MAE; higher is better for $R^2$.

| material | strain_type | model | $N_{\text{train}}$ | RMSE (eV) | MAE (eV) | $R^2$ |
|---|---|---|---|---|---|---|
| CsSnBr3 | isotropic | KRR_RBF_a0.0001_g0.5 | 14 | 0.07678 | 0.05845 | 0.99273 |
| CsSnBr3 | isotropic | KRR_RBF_a0.0001_g2.0 | 14 | 0.20064 | 0.11396 | 0.95036 |
| CsSnBr3 | isotropic | GPR_ls0.05_nl1e-06 | 14 | 0.23491 | 0.15182 | 0.93195 |
| CsSnBr3 | isotropic | GPR_ls0.05_nl0.0001 | 14 | 0.23493 | 0.15199 | 0.93194 |
| CsSnBr3 | isotropic | GPR_ls0.08_nl0.0001 | 14 | 0.23493 | 0.15199 | 0.93194 |
| CsSnBr3 | isotropic | GPR_ls0.03_nl1e-06 | 14 | 0.23493 | 0.15199 | 0.93194 |
| CsSnBr3 | isotropic | GPR_ls0.03_nl0.0001 | 14 | 0.23493 | 0.15199 | 0.93194 |
| CsSnBr3 | isotropic | KRR_RBF_a0.01_g0.5 | 14 | 0.25893 | 0.19169 | 0.91732 |
| CsSnBr3 | isotropic | KRR_RBF_a0.01_g2.0 | 14 | 0.30931 | 0.17168 | 0.88202 |
| CsSnBr3 | isotropic | SVR_RBF_C10_gscale | 14 | 0.35091 | 0.20204 | 0.84815 |
| CsSnBr3 | isotropic | SVR_RBF_C10_g1.0 | 14 | 0.35091 | 0.20204 | 0.84815 |
| CsSnBr3 | isotropic | SVR_RBF_C100_gscale | 14 | 0.35091 | 0.20204 | 0.84815 |
| CsSnBr3 | isotropic | SVR_RBF_C100_g1.0 | 14 | 0.35091 | 0.20204 | 0.84815 |
| CsSnBr3 | isotropic | kNN_k2 | 14 | 0.41733 | 0.26196 | 0.78522 |
| CsSnBr3 | isotropic | kNN_k3 | 14 | 0.44715 | 0.34519 | 0.75344 |
| CsSnBr3 | isotropic | RF_n300_dNone_leaf1 | 14 | 0.44956 | 0.32321 | 0.75078 |
| CsSnBr3 | isotropic | RF_n300_d4_leaf1 | 14 | 0.45901 | 0.34438 | 0.74018 |
| CsSnBr3 | isotropic | SVR_RBF_C1_gscale | 14 | 0.47344 | 0.31264 | 0.72359 |
| CsSnBr3 | isotropic | SVR_RBF_C1_g1.0 | 14 | 0.47344 | 0.31264 | 0.72359 |
| CsSnBr3 | isotropic | RF_n300_dNone_leaf2 | 14 | 0.50003 | 0.40765 | 0.69167 |
| CsSnBr3 | isotropic | RF_n300_d4_leaf2 | 14 | 0.50003 | 0.40765 | 0.69167 |
| CsSnBr3 | isotropic | SVR_RBF_C10_g5.0 | 14 | 0.52583 | 0.31297 | 0.65902 |
| CsSnBr3 | isotropic | SVR_RBF_C100_g5.0 | 14 | 0.52583 | 0.31297 | 0.65902 |

Continued on next page

Table S1: Model benchmarking by material and loading mode. For each curve we list the algorithm, training size $N_{\text{train}}$, and leave-one-out cross-validation metrics (RMSE, MAE, $R^2$). Lower is better for RMSE/MAE; higher is better for $R^2$. (Continued)

| material | strain_type | model | $N_{\text{train}}$ | RMSE (eV) | MAE (eV) | $R^2$ |
|---|---|---|---|---|---|---|
| CsSnBr3 | isotropic | kNN_k4 | 14 | 0.53201 | 0.44238 | 0.65097 |
| CsSnBr3 | isotropic | GBDT_n300_lr0.05_d2 | 14 | 0.53702 | 0.41339 | 0.64436 |
| CsSnBr3 | isotropic | GBDT_n300_lr0.1_d3 | 14 | 0.5371 | 0.41343 | 0.64425 |
| CsSnBr3 | isotropic | GBDT_n300_lr0.1_d2 | 14 | 0.5371 | 0.41343 | 0.64425 |
| CsSnBr3 | isotropic | GBDT_n300_lr0.05_d3 | 14 | 0.5371 | 0.41343 | 0.64425 |
| CsSnBr3 | isotropic | SVR_RBF_C1_g5.0 | 14 | 0.54071 | 0.31936 | 0.63945 |
| CsSnBr3 | isotropic | kNN_k5 | 14 | 0.57381 | 0.46959 | 0.59397 |
| CsSnBr3 | isotropic | QuadRidge_a0.01 | 14 | 0.57835 | 0.52304 | 0.58752 |
| CsSnBr3 | isotropic | QuadRidge_a0.0001 | 14 | 0.65976 | 0.53392 | 0.46322 |
| CsSnBr3 | isotropic | KRR_RBF_a1.0_g0.5 | 14 | 0.66215 | 0.57364 | 0.45932 |
| CsSnBr3 | isotropic | KRR_RBF_a1.0_g2.0 | 14 | 0.73299 | 0.55123 | 0.33745 |
| CsSnBr3 | isotropic | GPR_ls0.08_nl1e-06 | 14 | 0.79699 | 0.49035 | 0.21669 |
| CsSnBr3 | isotropic | QuadRidge_a1.0 | 14 | 0.8635 | 0.69904 | 0.08051 |
| CsSnBr3 | isotropic | KRR_RBF_a0.0001_g10.0 | 14 | 0.91413 | 0.55913 | -0.03049 |
| CsSnBr3 | isotropic | KRR_RBF_a0.01_g10.0 | 14 | 0.92329 | 0.57164 | -0.05123 |
| CsSnBr3 | isotropic | QuadRidge_a10.0 | 14 | 0.95631 | 0.77268 | -0.12778 |
| CsSnBr3 | isotropic | KRR_RBF_a1.0_g10.0 | 14 | 1.2239 | 0.91061 | -0.8472 |
| CsSnBr3 | uniaxial_c | GPR_ls0.03_nl1e-06 | 11 | 0.02518 | 0.01949 | 0.99808 |
| CsSnBr3 | uniaxial_c | GPR_ls0.08_nl1e-06 | 11 | 0.02518 | 0.01949 | 0.99808 |
| CsSnBr3 | uniaxial_c | GPR_ls0.05_nl0.0001 | 11 | 0.02518 | 0.01949 | 0.99808 |
| CsSnBr3 | uniaxial_c | GPR_ls0.05_nl1e-06 | 11 | 0.02518 | 0.01949 | 0.99808 |
| CsSnBr3 | uniaxial_c | GPR_ls0.08_nl0.0001 | 11 | 0.02518 | 0.01949 | 0.99808 |
| CsSnBr3 | uniaxial_c | GPR_ls0.03_nl0.0001 | 11 | 0.02518 | 0.01949 | 0.99808 |
| CsSnBr3 | uniaxial_c | KRR_RBF_a0.01_g0.5 | 11 | 0.04106 | 0.02701 | 0.9949 |
| CsSnBr3 | uniaxial_c | KRR_RBF_a0.0001_g0.5 | 11 | 0.04561 | 0.03557 | 0.99371 |
| CsSnBr3 | uniaxial_c | kNN_k2 | 11 | 0.05612 | 0.03986 | 0.99047 |
| CsSnBr3 | uniaxial_c | KRR_RBF_a0.0001_g2.0 | 11 | 0.09023 | 0.07973 | 0.97537 |
| CsSnBr3 | uniaxial_c | RF_n300_dNone_leaf1 | 11 | 0.09503 | 0.08068 | 0.97268 |
| CsSnBr3 | uniaxial_c | RF_n300_d4_leaf1 | 11 | 0.09503 | 0.08068 | 0.97268 |
| CsSnBr3 | uniaxial_c | KRR_RBF_a0.01_g2.0 | 11 | 0.11749 | 0.06812 | 0.95824 |
| CsSnBr3 | uniaxial_c | SVR_RBF_C1_gscale | 11 | 0.12678 | 0.10571 | 0.95136 |
| CsSnBr3 | uniaxial_c | SVR_RBF_C1_g1.0 | 11 | 0.12678 | 0.10571 | 0.95136 |
| CsSnBr3 | uniaxial_c | SVR_RBF_C10_gscale | 11 | 0.12678 | 0.10571 | 0.95136 |
| CsSnBr3 | uniaxial_c | SVR_RBF_C10_g1.0 | 11 | 0.12678 | 0.10571 | 0.95136 |
| CsSnBr3 | uniaxial_c | SVR_RBF_C100_gscale | 11 | 0.12678 | 0.10571 | 0.95136 |

Continued on next page

Table S1: Model benchmarking by material and loading mode. For each curve we list the algorithm, training size $N_{train}$, and leave-one-out cross-validation metrics (RMSE, MAE, $R^2$). Lower is better for RMSE/MAE; higher is better for $R^2$. (Continued)

| material | strain_type | model | $N_{train}$ | RMSE (eV) | MAE (eV) | $R^2$ |
|---|---|---|---|---|---|---|
| CsSnBr3 | uniaxial_c | SVR_RBF_C100_g1.0 | 11 | 0.12678 | 0.10571 | 0.95136 |
| CsSnBr3 | uniaxial_c | QuadRidge_a0.01 | 11 | 0.13644 | 0.1133 | 0.94367 |
| CsSnBr3 | uniaxial_c | kNN_k3 | 11 | 0.14124 | 0.12715 | 0.93964 |
| CsSnBr3 | uniaxial_c | kNN_k4 | 11 | 0.15467 | 0.11618 | 0.92762 |
| CsSnBr3 | uniaxial_c | QuadRidge_a0.0001 | 11 | 0.15987 | 0.12723 | 0.92267 |
| CsSnBr3 | uniaxial_c | GBDT_n300_lr0.05_d3 | 11 | 0.16934 | 0.13773 | 0.91323 |
| CsSnBr3 | uniaxial_c | GBDT_n300_lr0.1_d2 | 11 | 0.16934 | 0.13773 | 0.91323 |
| CsSnBr3 | uniaxial_c | GBDT_n300_lr0.1_d3 | 11 | 0.16934 | 0.13773 | 0.91323 |
| CsSnBr3 | uniaxial_c | GBDT_n300_lr0.05_d2 | 11 | 0.16934 | 0.13773 | 0.91323 |
| CsSnBr3 | uniaxial_c | RF_n300_dNone_leaf2 | 11 | 0.17927 | 0.14787 | 0.90276 |
| CsSnBr3 | uniaxial_c | RF_n300_d4_leaf2 | 11 | 0.17927 | 0.14787 | 0.90276 |
| CsSnBr3 | uniaxial_c | kNN_k5 | 11 | 0.23795 | 0.20524 | 0.82868 |
| CsSnBr3 | uniaxial_c | SVR_RBF_C1_g5.0 | 11 | 0.24595 | 0.19444 | 0.81697 |
| CsSnBr3 | uniaxial_c | SVR_RBF_C10_g5.0 | 11 | 0.24595 | 0.19444 | 0.81697 |
| CsSnBr3 | uniaxial_c | SVR_RBF_C100_g5.0 | 11 | 0.24595 | 0.19444 | 0.81697 |
| CsSnBr3 | uniaxial_c | KRR_RBF_a1.0_g0.5 | 11 | 0.26494 | 0.17066 | 0.78761 |
| CsSnBr3 | uniaxial_c | KRR_RBF_a1.0_g2.0 | 11 | 0.36171 | 0.24115 | 0.60413 |
| CsSnBr3 | uniaxial_c | KRR_RBF_a0.0001_g10.0 | 11 | 0.45052 | 0.3056 | 0.38586 |
| CsSnBr3 | uniaxial_c | KRR_RBF_a0.01_g10.0 | 11 | 0.454 | 0.30885 | 0.37635 |
| CsSnBr3 | uniaxial_c | QuadRidge_a1.0 | 11 | 0.51872 | 0.47036 | 0.18587 |
| CsSnBr3 | uniaxial_c | QuadRidge_a10.0 | 11 | 0.61867 | 0.55982 | -0.1581 |
| CsSnBr3 | uniaxial_c | KRR_RBF_a1.0_g10.0 | 11 | 0.63994 | 0.46932 | -0.23909 |
| CsSnCl3 | isotropic | kNN_k2 | 15 | 0.43703 | 0.31043 | 0.81783 |
| CsSnCl3 | isotropic | KRR_RBF_a0.01_g0.5 | 15 | 0.46507 | 0.3527 | 0.79371 |
| CsSnCl3 | isotropic | SVR_RBF_C10_g1.0 | 15 | 0.47758 | 0.31191 | 0.78246 |
| CsSnCl3 | isotropic | SVR_RBF_C10_gscale | 15 | 0.47758 | 0.31191 | 0.78246 |
| CsSnCl3 | isotropic | kNN_k3 | 15 | 0.48596 | 0.38073 | 0.77476 |
| CsSnCl3 | isotropic | RF_n300_dNone_leaf1 | 15 | 0.50495 | 0.38162 | 0.75681 |
| CsSnCl3 | isotropic | RF_n300_d4_leaf1 | 15 | 0.51026 | 0.39871 | 0.75167 |
| CsSnCl3 | isotropic | SVR_RBF_C10_g5.0 | 15 | 0.55437 | 0.39204 | 0.70688 |
| CsSnCl3 | isotropic | GPR_ls0.03_nl0.0001 | 15 | 0.56866 | 0.39086 | 0.69157 |
| CsSnCl3 | isotropic | QuadRidge_a0.01 | 15 | 0.57197 | 0.49982 | 0.68798 |
| CsSnCl3 | isotropic | RF_n300_dNone_leaf2 | 15 | 0.59451 | 0.49857 | 0.66289 |
| CsSnCl3 | isotropic | RF_n300_d4_leaf2 | 15 | 0.59451 | 0.49857 | 0.66289 |
| CsSnCl3 | isotropic | QuadRidge_a0.0001 | 15 | 0.59817 | 0.50648 | 0.65873 |

Continued on next page

Table S1: Model benchmarking by material and loading mode. For each curve we list the algorithm, training size $N_{\text{train}}$, and leave-one-out cross-validation metrics (RMSE, MAE, $R^2$). Lower is better for RMSE/MAE; higher is better for $R^2$. (Continued)

| material | strain_type | model | $N_{\text{train}}$ | RMSE (eV) | MAE (eV) | $R^2$ |
|---|---|---|---|---|---|---|
| CsSnCl3 | isotropic | kNN_k4 | 15 | 0.60646 | 0.51405 | 0.64921 |
| CsSnCl3 | isotropic | kNN_k5 | 15 | 0.64898 | 0.56484 | 0.5983 |
| CsSnCl3 | isotropic | GBDT_n300_lr0.05_d2 | 15 | 0.66022 | 0.45703 | 0.58425 |
| CsSnCl3 | isotropic | GBDT_n300_lr0.1_d2 | 15 | 0.6606 | 0.4572 | 0.58378 |
| CsSnCl3 | isotropic | GBDT_n300_lr0.05_d3 | 15 | 0.6606 | 0.4572 | 0.58377 |
| CsSnCl3 | isotropic | GBDT_n300_lr0.1_d3 | 15 | 0.6606 | 0.4572 | 0.58377 |
| CsSnCl3 | isotropic | SVR_RBF_C1_g1.0 | 15 | 0.68347 | 0.47933 | 0.55446 |
| CsSnCl3 | isotropic | SVR_RBF_C1_gscale | 15 | 0.68347 | 0.47933 | 0.55446 |
| CsSnCl3 | isotropic | SVR_RBF_C1_g5.0 | 15 | 0.68637 | 0.46084 | 0.55067 |
| CsSnCl3 | isotropic | KRR_RBF_a1.0_g0.5 | 15 | 0.72033 | 0.60069 | 0.50511 |
| CsSnCl3 | isotropic | KRR_RBF_a0.01_g2.0 | 15 | 0.73981 | 0.43108 | 0.47798 |
| CsSnCl3 | isotropic | SVR_RBF_C100_g1.0 | 15 | 0.80791 | 0.44205 | 0.37745 |
| CsSnCl3 | isotropic | SVR_RBF_C100_gscale | 15 | 0.80791 | 0.44205 | 0.37745 |
| CsSnCl3 | isotropic | KRR_RBF_a1.0_g2.0 | 15 | 0.82379 | 0.61771 | 0.35274 |
| CsSnCl3 | isotropic | SVR_RBF_C100_g5.0 | 15 | 0.89688 | 0.63009 | 0.23279 |
| CsSnCl3 | isotropic | GPR_ls0.03_nl1e-06 | 15 | 0.9076 | 0.7244 | 0.21433 |
| CsSnCl3 | isotropic | QuadRidge_a1.0 | 15 | 0.94068 | 0.7869 | 0.15602 |
| CsSnCl3 | isotropic | QuadRidge_a10.0 | 15 | 1.07704 | 0.87098 | -0.1064 |
| CsSnCl3 | isotropic | GPR_ls0.08_nl1e-06 | 15 | 1.09708 | 0.88437 | -0.14796 |
| CsSnCl3 | isotropic | GPR_ls0.08_nl0.0001 | 15 | 1.09708 | 0.88437 | -0.14796 |
| CsSnCl3 | isotropic | KRR_RBF_a0.01_g10.0 | 15 | 1.10595 | 0.86211 | -0.16659 |
| CsSnCl3 | isotropic | GPR_ls0.05_nl0.0001 | 15 | 1.12045 | 0.93598 | -0.19737 |
| CsSnCl3 | isotropic | GPR_ls0.05_nl1e-06 | 15 | 1.12045 | 0.93598 | -0.19737 |
| CsSnCl3 | isotropic | KRR_RBF_a0.0001_g10.0 | 15 | 1.12952 | 0.91842 | -0.21685 |
| CsSnCl3 | isotropic | KRR_RBF_a1.0_g10.0 | 15 | 1.31873 | 0.97613 | -0.65866 |
| CsSnCl3 | isotropic | KRR_RBF_a0.0001_g0.5 | 15 | 1.43474 | 0.61922 | -0.96333 |
| CsSnCl3 | isotropic | KRR_RBF_a0.0001_g2.0 | 15 | 2.20638 | 0.87084 | -3.64312 |
| CsSnCl3 | uniaxial_c | GPR_ls0.05_nl1e-06 | 11 | 0.04826 | 0.03294 | 0.99473 |
| CsSnCl3 | uniaxial_c | GPR_ls0.03_nl1e-06 | 11 | 0.04826 | 0.03294 | 0.99473 |
| CsSnCl3 | uniaxial_c | GPR_ls0.08_nl0.0001 | 11 | 0.04826 | 0.03294 | 0.99473 |
| CsSnCl3 | uniaxial_c | GPR_ls0.03_nl0.0001 | 11 | 0.04826 | 0.03294 | 0.99473 |
| CsSnCl3 | uniaxial_c | GPR_ls0.08_nl1e-06 | 11 | 0.04826 | 0.03294 | 0.99473 |
| CsSnCl3 | uniaxial_c | GPR_ls0.05_nl0.0001 | 11 | 0.04826 | 0.03294 | 0.99473 |
| CsSnCl3 | uniaxial_c | KRR_RBF_a0.0001_g0.5 | 11 | 0.04935 | 0.03727 | 0.99449 |
| CsSnCl3 | uniaxial_c | KRR_RBF_a0.01_g0.5 | 11 | 0.05908 | 0.03886 | 0.9921 |

Continued on next page

Table S1: Model benchmarking by material and loading mode. For each curve we list the algorithm, training size $N_{\text{train}}$, and leave-one-out cross-validation metrics (RMSE, MAE, $R^2$). Lower is better for RMSE/MAE; higher is better for $R^2$. (Continued)

| material | strain_type | model | $N_{\text{train}}$ | RMSE (eV) | MAE (eV) | $R^2$ |
|---|---|---|---|---|---|---|
| CsSnCl3 | uniaxial_c | kNN_k2 | 11 | 0.07257 | 0.054 | 0.98808 |
| CsSnCl3 | uniaxial_c | KRR_RBF_a0.0001_g2.0 | 11 | 0.10715 | 0.09738 | 0.974 |
| CsSnCl3 | uniaxial_c | RF_n300_dNone_leaf1 | 11 | 0.10893 | 0.09348 | 0.97313 |
| CsSnCl3 | uniaxial_c | RF_n300_d4_leaf1 | 11 | 0.10893 | 0.09348 | 0.97313 |
| CsSnCl3 | uniaxial_c | QuadRidge_a0.01 | 11 | 0.1144 | 0.10425 | 0.97037 |
| CsSnCl3 | uniaxial_c | SVR_RBF_C1_gscale | 11 | 0.13288 | 0.1095 | 0.96002 |
| CsSnCl3 | uniaxial_c | SVR_RBF_C1_g1.0 | 11 | 0.13288 | 0.1095 | 0.96002 |
| CsSnCl3 | uniaxial_c | SVR_RBF_C10_gscale | 11 | 0.13288 | 0.1095 | 0.96002 |
| CsSnCl3 | uniaxial_c | SVR_RBF_C10_g1.0 | 11 | 0.13288 | 0.1095 | 0.96002 |
| CsSnCl3 | uniaxial_c | SVR_RBF_C100_gscale | 11 | 0.13288 | 0.1095 | 0.96002 |
| CsSnCl3 | uniaxial_c | SVR_RBF_C100_g1.0 | 11 | 0.13288 | 0.1095 | 0.96002 |
| CsSnCl3 | uniaxial_c | QuadRidge_a0.0001 | 11 | 0.14881 | 0.1171 | 0.94986 |
| CsSnCl3 | uniaxial_c | KRR_RBF_a0.01_g2.0 | 11 | 0.15249 | 0.08413 | 0.94735 |
| CsSnCl3 | uniaxial_c | kNN_k3 | 11 | 0.17279 | 0.15821 | 0.9324 |
| CsSnCl3 | uniaxial_c | GBDT_n300_lr0.1_d3 | 11 | 0.19032 | 0.16318 | 0.91798 |
| CsSnCl3 | uniaxial_c | GBDT_n300_lr0.1_d2 | 11 | 0.19032 | 0.16318 | 0.91798 |
| CsSnCl3 | uniaxial_c | GBDT_n300_lr0.05_d3 | 11 | 0.19032 | 0.16318 | 0.91798 |
| CsSnCl3 | uniaxial_c | GBDT_n300_lr0.05_d2 | 11 | 0.19032 | 0.16318 | 0.91798 |
| CsSnCl3 | uniaxial_c | kNN_k4 | 11 | 0.19116 | 0.142 | 0.91726 |
| CsSnCl3 | uniaxial_c | RF_n300_dNone_leaf2 | 11 | 0.21781 | 0.17952 | 0.89258 |
| CsSnCl3 | uniaxial_c | RF_n300_d4_leaf2 | 11 | 0.21781 | 0.17952 | 0.89258 |
| CsSnCl3 | uniaxial_c | SVR_RBF_C1_g5.0 | 11 | 0.27974 | 0.21936 | 0.82281 |
| CsSnCl3 | uniaxial_c | SVR_RBF_C10_g5.0 | 11 | 0.27974 | 0.21936 | 0.82281 |
| CsSnCl3 | uniaxial_c | SVR_RBF_C100_g5.0 | 11 | 0.27974 | 0.21936 | 0.82281 |
| CsSnCl3 | uniaxial_c | kNN_k5 | 11 | 0.2886 | 0.25045 | 0.8114 |
| CsSnCl3 | uniaxial_c | KRR_RBF_a1.0_g0.5 | 11 | 0.31869 | 0.20803 | 0.77003 |
| CsSnCl3 | uniaxial_c | KRR_RBF_a1.0_g2.0 | 11 | 0.44603 | 0.31217 | 0.54953 |
| CsSnCl3 | uniaxial_c | KRR_RBF_a0.0001_g10.0 | 11 | 0.55606 | 0.39382 | 0.29987 |
| CsSnCl3 | uniaxial_c | KRR_RBF_a0.01_g10.0 | 11 | 0.56051 | 0.39831 | 0.28862 |
| CsSnCl3 | uniaxial_c | QuadRidge_a1.0 | 11 | 0.59682 | 0.5387 | 0.19344 |
| CsSnCl3 | uniaxial_c | QuadRidge_a10.0 | 11 | 0.71487 | 0.64301 | -0.15715 |
| CsSnCl3 | uniaxial_c | KRR_RBF_a1.0_g10.0 | 11 | 0.79849 | 0.61816 | -0.44373 |
| CsSnI3 | isotropic | KRR_RBF_a0.0001_g2.0 | 14 | 0.14854 | 0.07829 | 0.96384 |
| CsSnI3 | isotropic | SVR_RBF_C10_gscale | 14 | 0.20417 | 0.14144 | 0.93168 |
| CsSnI3 | isotropic | SVR_RBF_C100_gscale | 14 | 0.20417 | 0.14144 | 0.93168 |

Continued on next page

Table S1: Model benchmarking by material and loading mode. For each curve we list the algorithm, training size $N_{\mathrm{train}}$, and leave-one-out cross-validation metrics (RMSE, MAE, $R^2$). Lower is better for RMSE/MAE; higher is better for $R^2$. (Continued)

| material | strain_type | model | $N_{\mathrm{train}}$ | RMSE (eV) | MAE (eV) | $R^2$ |
|---|---|---|---|---|---|---|
| CsSnI3 | isotropic | SVR_RBF_C10_g1.0 | 14 | 0.20417 | 0.14144 | 0.93168 |
| CsSnI3 | isotropic | SVR_RBF_C100_g1.0 | 14 | 0.20417 | 0.14144 | 0.93168 |
| CsSnI3 | isotropic | KRR_RBF_a0.01_g0.5 | 14 | 0.20424 | 0.17659 | 0.93163 |
| CsSnI3 | isotropic | KRR_RBF_a0.0001_g0.5 | 14 | 0.21657 | 0.12577 | 0.92313 |
| CsSnI3 | isotropic | GPR_ls0.08_nl0.0001 | 14 | 0.22725 | 0.1314 | 0.91536 |
| CsSnI3 | isotropic | GPR_ls0.05_nl0.0001 | 14 | 0.22792 | 0.13355 | 0.91486 |
| CsSnI3 | isotropic | GPR_ls0.05_nl1e-06 | 14 | 0.22792 | 0.13355 | 0.91486 |
| CsSnI3 | isotropic | GPR_ls0.03_nl0.0001 | 14 | 0.22804 | 0.1342 | 0.91477 |
| CsSnI3 | isotropic | GPR_ls0.03_nl1e-06 | 14 | 0.22804 | 0.1342 | 0.91477 |
| CsSnI3 | isotropic | KRR_RBF_a0.01_g2.0 | 14 | 0.24641 | 0.13577 | 0.90049 |
| CsSnI3 | isotropic | kNN_k2 | 14 | 0.3657 | 0.22557 | 0.78082 |
| CsSnI3 | isotropic | RF_n300_dNone_leaf1 | 14 | 0.37435 | 0.26655 | 0.77032 |
| CsSnI3 | isotropic | RF_n300_d4_leaf1 | 14 | 0.38192 | 0.28177 | 0.76095 |
| CsSnI3 | isotropic | kNN_k3 | 14 | 0.409 | 0.29133 | 0.72584 |
| CsSnI3 | isotropic | SVR_RBF_C10_g5.0 | 14 | 0.42049 | 0.25814 | 0.71022 |
| CsSnI3 | isotropic | SVR_RBF_C100_g5.0 | 14 | 0.42049 | 0.25814 | 0.71022 |
| CsSnI3 | isotropic | SVR_RBF_C1_g5.0 | 14 | 0.42105 | 0.25709 | 0.70945 |
| CsSnI3 | isotropic | GBDT_n300_lr0.05_d2 | 14 | 0.42912 | 0.34209 | 0.6982 |
| CsSnI3 | isotropic | GBDT_n300_lr0.1_d3 | 14 | 0.42912 | 0.34207 | 0.6982 |
| CsSnI3 | isotropic | GBDT_n300_lr0.1_d2 | 14 | 0.42912 | 0.34207 | 0.6982 |
| CsSnI3 | isotropic | GBDT_n300_lr0.05_d3 | 14 | 0.42913 | 0.34207 | 0.6982 |
| CsSnI3 | isotropic | SVR_RBF_C1_gscale | 14 | 0.46257 | 0.33269 | 0.64933 |
| CsSnI3 | isotropic | SVR_RBF_C1_g1.0 | 14 | 0.46257 | 0.33269 | 0.64933 |
| CsSnI3 | isotropic | RF_n300_dNone_leaf2 | 14 | 0.46376 | 0.37373 | 0.64752 |
| CsSnI3 | isotropic | RF_n300_d4_leaf2 | 14 | 0.46376 | 0.37373 | 0.64752 |
| CsSnI3 | isotropic | kNN_k4 | 14 | 0.49975 | 0.41559 | 0.59069 |
| CsSnI3 | isotropic | kNN_k5 | 14 | 0.53486 | 0.44174 | 0.53114 |
| CsSnI3 | isotropic | QuadRidge_a0.01 | 14 | 0.56592 | 0.51581 | 0.47511 |
| CsSnI3 | isotropic | KRR_RBF_a1.0_g0.5 | 14 | 0.60764 | 0.54105 | 0.39488 |
| CsSnI3 | isotropic | KRR_RBF_a1.0_g2.0 | 14 | 0.62858 | 0.48724 | 0.35244 |
| CsSnI3 | isotropic | QuadRidge_a0.0001 | 14 | 0.64374 | 0.5338 | 0.32084 |
| CsSnI3 | isotropic | GPR_ls0.08_nl1e-06 | 14 | 0.73945 | 0.50152 | 0.10388 |
| CsSnI3 | isotropic | QuadRidge_a1.0 | 14 | 0.76272 | 0.64943 | 0.04657 |
| CsSnI3 | isotropic | KRR_RBF_a0.0001_g10.0 | 14 | 0.76932 | 0.46642 | 0.03 |
| CsSnI3 | isotropic | KRR_RBF_a0.01_g10.0 | 14 | 0.77767 | 0.4795 | 0.00883 |

Continued on next page

Table S1: Model benchmarking by material and loading mode. For each curve we list the algorithm, training size $N_{\text{train}}$, and leave-one-out cross-validation metrics (RMSE, MAE, $R^2$). Lower is better for RMSE/MAE; higher is better for $R^2$. (Continued)

| material | strain_type | model | $N_{\text{train}}$ | RMSE (eV) | MAE (eV) | $R^2$ |
|---|---|---|---|---|---|---|
| CsSnI3 | isotropic | QuadRidge_a10.0 | 14 | 0.8312 | 0.69572 | -0.13231 |
| CsSnI3 | isotropic | KRR_RBF_a1.0_g10.0 | 14 | 1.05145 | 0.78669 | -0.81189 |
| CsSnI3 | uniaxial_c | kNN_k2 | 11 | 0.04288 | 0.03068 | 0.99146 |
| CsSnI3 | uniaxial_c | KRR_RBF_a0.01_g0.5 | 11 | 0.04541 | 0.03703 | 0.99042 |
| CsSnI3 | uniaxial_c | GPR_ls0.03_nl0.0001 | 11 | 0.04952 | 0.038 | 0.98861 |
| CsSnI3 | uniaxial_c | GPR_ls0.05_nl0.0001 | 11 | 0.04952 | 0.038 | 0.98861 |
| CsSnI3 | uniaxial_c | GPR_ls0.08_nl0.0001 | 11 | 0.04952 | 0.03801 | 0.98861 |
| CsSnI3 | uniaxial_c | GPR_ls0.03_nl1e-06 | 11 | 0.04952 | 0.03801 | 0.98861 |
| CsSnI3 | uniaxial_c | GPR_ls0.08_nl1e-06 | 11 | 0.04952 | 0.03801 | 0.98861 |
| CsSnI3 | uniaxial_c | GPR_ls0.05_nl1e-06 | 11 | 0.04952 | 0.03801 | 0.98861 |
| CsSnI3 | uniaxial_c | KRR_RBF_a0.0001_g0.5 | 11 | 0.06896 | 0.05315 | 0.97791 |
| CsSnI3 | uniaxial_c | KRR_RBF_a0.0001_g2.0 | 11 | 0.07744 | 0.04499 | 0.97215 |
| CsSnI3 | uniaxial_c | RF_n300_dNone_leaf1 | 11 | 0.07924 | 0.06113 | 0.97084 |
| CsSnI3 | uniaxial_c | RF_n300_d4_leaf1 | 11 | 0.07924 | 0.06113 | 0.97084 |
| CsSnI3 | uniaxial_c | KRR_RBF_a0.01_g2.0 | 11 | 0.09819 | 0.05758 | 0.95523 |
| CsSnI3 | uniaxial_c | SVR_RBF_C1_gscale | 11 | 0.11701 | 0.09645 | 0.93641 |
| CsSnI3 | uniaxial_c | SVR_RBF_C1_g1.0 | 11 | 0.11701 | 0.09645 | 0.93641 |
| CsSnI3 | uniaxial_c | SVR_RBF_C10_gscale | 11 | 0.11701 | 0.09645 | 0.93641 |
| CsSnI3 | uniaxial_c | SVR_RBF_C10_g1.0 | 11 | 0.11701 | 0.09645 | 0.93641 |
| CsSnI3 | uniaxial_c | SVR_RBF_C100_gscale | 11 | 0.11701 | 0.09645 | 0.93641 |
| CsSnI3 | uniaxial_c | SVR_RBF_C100_g1.0 | 11 | 0.11701 | 0.09645 | 0.93641 |
| CsSnI3 | uniaxial_c | kNN_k4 | 11 | 0.11755 | 0.0913 | 0.93583 |
| CsSnI3 | uniaxial_c | kNN_k3 | 11 | 0.11971 | 0.09576 | 0.93345 |
| CsSnI3 | uniaxial_c | RF_n300_dNone_leaf2 | 11 | 0.14113 | 0.12064 | 0.9075 |
| CsSnI3 | uniaxial_c | RF_n300_d4_leaf2 | 11 | 0.14113 | 0.12064 | 0.9075 |
| CsSnI3 | uniaxial_c | QuadRidge_a0.01 | 11 | 0.14224 | 0.12167 | 0.90605 |
| CsSnI3 | uniaxial_c | GBDT_n300_lr0.05_d3 | 11 | 0.14657 | 0.11264 | 0.90023 |
| CsSnI3 | uniaxial_c | GBDT_n300_lr0.1_d3 | 11 | 0.14657 | 0.11264 | 0.90023 |
| CsSnI3 | uniaxial_c | GBDT_n300_lr0.1_d2 | 11 | 0.14657 | 0.11264 | 0.90023 |
| CsSnI3 | uniaxial_c | GBDT_n300_lr0.05_d2 | 11 | 0.14657 | 0.11264 | 0.90023 |
| CsSnI3 | uniaxial_c | QuadRidge_a0.0001 | 11 | 0.16586 | 0.13181 | 0.87224 |
| CsSnI3 | uniaxial_c | kNN_k5 | 11 | 0.18394 | 0.16118 | 0.84287 |
| CsSnI3 | uniaxial_c | SVR_RBF_C1_g5.0 | 11 | 0.20039 | 0.16508 | 0.81352 |
| CsSnI3 | uniaxial_c | SVR_RBF_C10_g5.0 | 11 | 0.20039 | 0.16508 | 0.81352 |
| CsSnI3 | uniaxial_c | SVR_RBF_C100_g5.0 | 11 | 0.20039 | 0.16508 | 0.81352 |

Continued on next page

Table S1: Model benchmarking by material and loading mode. For each curve we list the algorithm, training size $N_{\text{train}}$, and leave-one-out cross-validation metrics (RMSE, MAE, $R^2$). Lower is better for RMSE/MAE; higher is better for $R^2$. (Continued)

| material | strain_type | model | $N_{\text{train}}$ | RMSE (eV) | MAE (eV) | $R^2$ |
|---|---|---|---|---|---|---|
| CsSnI3 | uniaxial_c | KRR_RBF_a1.0_g0.5 | 11 | 0.20671 | 0.14419 | 0.80156 |
| CsSnI3 | uniaxial_c | KRR_RBF_a1.0_g2.0 | 11 | 0.279 | 0.18789 | 0.6385 |
| CsSnI3 | uniaxial_c | KRR_RBF_a0.0001_g10.0 | 11 | 0.34826 | 0.23339 | 0.43674 |
| CsSnI3 | uniaxial_c | KRR_RBF_a0.01_g10.0 | 11 | 0.35098 | 0.23581 | 0.42793 |
| CsSnI3 | uniaxial_c | QuadRidge_a1.0 | 11 | 0.42115 | 0.38707 | 0.17632 |
| CsSnI3 | uniaxial_c | KRR_RBF_a1.0_g10.0 | 11 | 0.49602 | 0.35486 | -0.1426 |
| CsSnI3 | uniaxial_c | QuadRidge_a10.0 | 11 | 0.49964 | 0.45841 | -0.1593 |

Table S2: Best-performing model per material and loading mode with leave-one-out metrics.

| material | strain_type | best_model | $\text{RMSE}_{\text{best}}$ (eV) | $\text{MAE}_{\text{best}}$ (eV) | $R^2_{\text{best}}$ | $N_{\text{train}}$ |
|---|---|---|---|---|---|---|
| CsSnCl3 | isotropic | kNN_k2 | 0.437033465538 | 0.310433333333 | 0.817829894665 | 15 |
| CsSnCl3 | uniaxial_c | GPR_ls0.05_nl1e-06 | 0.0482568159661 | 0.0329363649878 | 0.994726999057 | 11 |
| CsSnBr3 | isotropic | KRR_RBF_a0.0001_g0.5 | 0.0767757956038 | 0.0584516691977 | 0.99273102596 | 14 |
| CsSnBr3 | uniaxial_c | GPR_ls0.03_nl1e-06 | 0.0251788180405 | 0.0194886439951 | 0.998081772725 | 11 |
| CsSnI3 | isotropic | KRR_RBF_a0.0001_g2.0 | 0.14853537786 | 0.0782872728848 | 0.963841143906 | 14 |
| CsSnI3 | uniaxial_c | kNN_k2 | 0.0428779981724 | 0.0306818181818 | 0.991461966356 | 11 |

Table S3: Deformation potentials at $\varepsilon = 0\%$ from the winner curves. $a_g = \mathrm{d}E_g/\mathrm{d}\varepsilon|_{\varepsilon=0}$. Uncertainties are propagated from the model's predictive variance.

| material | strain_type | $a_g$ (eV/%) | uncertainty (eV/%) |
|---|---|---|---|
| CsSnBr3 | isotropic | 0.102632 | 0.013953 |
| CsSnBr3 | uniaxial_c | 0.050505 | 0.006506 |
| CsSnCl3 | isotropic | 0.180200 | 0.068837 |
| CsSnCl3 | uniaxial_c | 0.052212 | 0.007909 |
| CsSnI3 | isotropic | 0.094694 | 0.014113 |
| CsSnI3 | uniaxial_c | 0.042600 | 0.039920 |

Table S4: Winner-model predictions on the tabulated strain grid. For each material and loading mode we report the strain $\varepsilon$ (%), predictive mean $\mu$ (eV), and predictive uncertainty $\sigma$ (eV).

| material | strain_type | $\varepsilon$ (%) | $\mu$ (eV) | $\sigma$ (eV) |
|---|---|---|---|---|
| CsSnBr3 | uniaxial_c | -25.0 | 0.004198437015510148 | 0.02707042928562638 |
| CsSnBr3 | uniaxial_c | -22.5 | -0.0180000320902709 | 0.024098540687749328 |
| CsSnBr3 | uniaxial_c | -20.0 | -0.02280218228096209 | 0.023482663584247367 |
| CsSnBr3 | uniaxial_c | -17.5 | -0.008670482750615549 | 0.023531336917315394 |
| CsSnBr3 | uniaxial_c | -15.0 | 0.025184061106357736 | 0.023508004016674994 |
| CsSnBr3 | uniaxial_c | -12.5 | 0.07873086249789452 | 0.023316819282199006 |
| CsSnBr3 | uniaxial_c | -10.0 | 0.15109744257791258 | 0.023093449379446355 |
| CsSnBr3 | uniaxial_c | -7.5 | 0.2405979662165516 | 0.02296429006219494 |
| CsSnBr3 | uniaxial_c | -5.0 | 0.34481065347179557 | 0.022954376191273655 |
| CsSnBr3 | uniaxial_c | -2.5 | 0.46069824429638206 | 0.023002785168711994 |
| CsSnBr3 | uniaxial_c | 0.0 | 0.5847624552016893 | 0.02303039049025718 |
| CsSnBr3 | uniaxial_c | 2.5 | 0.7132210423623782 | 0.023002785168711994 |
| CsSnBr3 | uniaxial_c | 5.0 | 0.8421948632869125 | 0.022954376191272056 |
| CsSnBr3 | uniaxial_c | 7.5 | 0.9678922645488885 | 0.022964290062196534 |
| CsSnBr3 | uniaxial_c | 10.0 | 1.0867791419727872 | 0.023093449379446355 |
| CsSnBr3 | uniaxial_c | 12.5 | 1.1957249364988 | 0.023316819282199006 |
| CsSnBr3 | uniaxial_c | 15.0 | 1.2921173787066769 | 0.023508004016675778 |
| CsSnBr3 | uniaxial_c | 17.5 | 1.3739416728351985 | 0.023531336917314613 |
| CsSnBr3 | uniaxial_c | 20.0 | 1.43982271320588 | 0.023482663584247367 |
| CsSnBr3 | uniaxial_c | 22.5 | 1.4890315851789198 | 0.024098540687749328 |
| CsSnBr3 | uniaxial_c | 25.0 | 1.521459815260301 | 0.027070429285628417 |
| CsSnBr3 | isotropic | -25.0 | 0.0001925952424109978 | 0.30353284107456924 |
| CsSnBr3 | isotropic | -22.5 | 0.6782194276678801 | 0.1920387644754096 |
| CsSnBr3 | isotropic | -20.0 | 1.1850778094354535 | 0.13341340890832062 |
| CsSnBr3 | isotropic | -17.5 | 1.448860233139059 | 0.10164697604668077 |
| CsSnBr3 | isotropic | -15.0 | 1.4550193249472363 | 0.08209021639400738 |
| CsSnBr3 | isotropic | -12.5 | 1.2524042246969191 | 0.06998639098096271 |
| CsSnBr3 | isotropic | -10.0 | 0.940291160761948 | 0.0591130917114339 |
| CsSnBr3 | isotropic | -7.5 | 0.6395297166540139 | 0.05050694042589325 |
| CsSnBr3 | isotropic | -5.0 | 0.4570804009710976 | 0.04803014770923365 |
| CsSnBr3 | isotropic | -2.5 | 0.45614114478967593 | 0.045551637905119124 |
| CsSnBr3 | isotropic | 0.0 | 0.6422081361068663 | 0.0429014735360031 |
| CsSnBr3 | isotropic | 2.5 | 0.9692998973500053 | 0.05284258246973891 |
| CsSnBr3 | isotropic | 5.0 | 1.3626853937124253 | 0.06887429774230457 |
| CsSnBr3 | isotropic | 7.5 | 1.7481959094319137 | 0.08029027481360068 |
| CsSnBr3 | isotropic | 10.0 | 2.076277151997374 | 0.09637892506953769 |

Continued on next page

Table S4: Winner-model predictions on the tabulated strain grid. For each material and loading mode we report the strain $\varepsilon$ (%), predictive mean $\mu$ (eV), and predictive uncertainty $\sigma$ (eV). (Continued)

| material | strain_type | $\varepsilon$ (%) | $\mu$ (eV) | $\sigma$ (eV) |
|---|---|---|---|---|
| CsSnBr3 | isotropic | 12.5 | 2.3320709999869536 | 0.12830558807104922 |
| CsSnBr3 | isotropic | 15.0 | 2.529402866788317 | 0.17727531864660212 |
| CsSnBr3 | isotropic | 17.5 | 2.6934886106912614 | 0.24647491239084318 |
| CsSnBr3 | isotropic | 20.0 | 2.8413947846175347 | 0.33458080829382414 |
| CsSnBr3 | isotropic | 22.5 | 2.9691886212573593 | 0.43270529043631767 |
| CsSnBr3 | isotropic | 25.0 | 3.050794482570595 | 0.5354880277405438 |
| CsSnCl3 | uniaxial_c | -25.0 | -0.005181020836743433 | 0.03268283535182985 |
| CsSnCl3 | uniaxial_c | -22.5 | -0.01708914830601127 | 0.02900678050990843 |
| CsSnCl3 | uniaxial_c | -20.0 | 0.0032481320330517427 | 0.028791563723199663 |
| CsSnCl3 | uniaxial_c | -17.5 | 0.05510624401569297 | 0.02884642315923267 |
| CsSnCl3 | uniaxial_c | -15.0 | 0.13549866281117817 | 0.028539049551916884 |
| CsSnCl3 | uniaxial_c | -12.5 | 0.23959234918439054 | 0.028174213546215732 |
| CsSnCl3 | uniaxial_c | -10.0 | 0.36134812996558574 | 0.02800081362496955 |
| CsSnCl3 | uniaxial_c | -7.5 | 0.4942836313998581 | 0.027985946066624884 |
| CsSnCl3 | uniaxial_c | -5.0 | 0.6322344609416799 | 0.02799173023895309 |
| CsSnCl3 | uniaxial_c | -2.5 | 0.769990578678517 | 0.027963922291983138 |
| CsSnCl3 | uniaxial_c | 0.0 | 0.9037095536516085 | 0.027943437495043657 |
| CsSnCl3 | uniaxial_c | 2.5 | 1.0310519467884547 | 0.027963922291983138 |
| CsSnCl3 | uniaxial_c | 5.0 | 1.1510375473087695 | 0.027991730238953964 |
| CsSnCl3 | uniaxial_c | 7.5 | 1.2636735705090307 | 0.027985946066624006 |
| CsSnCl3 | uniaxial_c | 10.0 | 1.3694464696182895 | 0.028000813624968677 |
| CsSnCl3 | uniaxial_c | 12.5 | 1.4687897316747418 | 0.02817421354621486 |
| CsSnCl3 | uniaxial_c | 15.0 | 1.5616374205790344 | 0.028539049551917745 |
| CsSnCl3 | uniaxial_c | 17.5 | 1.6471489488995854 | 0.028846423159234368 |
| CsSnCl3 | uniaxial_c | 20.0 | 1.723650814695347 | 0.028791563723199663 |
| CsSnCl3 | uniaxial_c | 22.5 | 1.7887949754978845 | 0.029006780509905895 |
| CsSnCl3 | uniaxial_c | 25.0 | 1.8398910067386742 | 0.03268283535182985 |
| CsSnCl3 | isotropic | -25.0 | 0.0 | 0.4995734408222673 |
| CsSnCl3 | isotropic | -22.5 | 0.0 | 0.4995734408222673 |
| CsSnCl3 | isotropic | -20.0 | 0.7915 | 0.5397248201398556 |
| CsSnCl3 | isotropic | -17.5 | 1.524 | 0.46064322402891184 |
| CsSnCl3 | isotropic | -15.0 | 1.524 | 0.24709234760257137 |
| CsSnCl3 | isotropic | -12.5 | 1.0275 | 0.23088204227213083 |
| CsSnCl3 | isotropic | -10.0 | 1.0275 | 0.22442273212344135 |
| CsSnCl3 | isotropic | -7.5 | 0.7110000000000001 | 0.179132271241114 |
| CsSnCl3 | isotropic | -5.0 | 0.6385000000000001 | 0.1326129970770211 |

Continued on next page

Table S4: Winner-model predictions on the tabulated strain grid. For each material and loading mode we report the strain $\varepsilon$ (%), predictive mean $\mu$ (eV), and predictive uncertainty $\sigma$ (eV). (Continued)

| material | strain_type | $\varepsilon$ (%) | $\mu$ (eV) | $\sigma$ (eV) |
|---|---|---|---|---|
| CsSnCl3 | isotropic | -2.5 | 0.6385000000000001 | 0.19385898476727878 |
| CsSnCl3 | isotropic | 0.0 | 0.7945 | 0.2287276032614998 |
| CsSnCl3 | isotropic | 2.5 | 1.5394999999999999 | 0.28439647403536833 |
| CsSnCl3 | isotropic | 5.0 | 1.5394999999999999 | 0.3071889434757538 |
| CsSnCl3 | isotropic | 7.5 | 2.0469999999999997 | 0.34313718465615145 |
| CsSnCl3 | isotropic | 10.0 | 2.0469999999999997 | 0.3587232453786621 |
| CsSnCl3 | isotropic | 12.5 | 2.597 | 0.3314956761030225 |
| CsSnCl3 | isotropic | 15.0 | 2.597 | 0.2989434004853594 |
| CsSnCl3 | isotropic | 17.5 | 2.9935 | 0.29946976757888244 |
| CsSnCl3 | isotropic | 20.0 | 2.9935 | 0.31031569989286745 |
| CsSnCl3 | isotropic | 22.5 | 3.269 | 0.32582587595792645 |
| CsSnCl3 | isotropic | 25.0 | 3.269 | 0.33246118546944714 |
| CsSnI3 | uniaxial_c | -25.0 | 0.0 | 0.026131207396521125 |
| CsSnI3 | uniaxial_c | -22.5 | 0.0 | 0.026131207396521125 |
| CsSnI3 | uniaxial_c | -20.0 | 0.0 | 0.026131207396521125 |
| CsSnI3 | uniaxial_c | -17.5 | 0.0 | 0.026102336581233496 |
| CsSnI3 | uniaxial_c | -15.0 | 0.0015 | 0.034642073317715835 |
| CsSnI3 | uniaxial_c | -12.5 | 0.0015 | 0.055046150580671825 |
| CsSnI3 | uniaxial_c | -10.0 | 0.0015 | 0.09365885139029849 |
| CsSnI3 | uniaxial_c | -7.5 | 0.1005 | 0.11468940393515 |
| CsSnI3 | uniaxial_c | -5.0 | 0.1005 | 0.12383373810779505 |
| CsSnI3 | uniaxial_c | -2.5 | 0.316 | 0.13755091593660876 |
| CsSnI3 | uniaxial_c | 0.0 | 0.316 | 0.14115905831277709 |
| CsSnI3 | uniaxial_c | 2.5 | 0.529 | 0.14463906102778745 |
| CsSnI3 | uniaxial_c | 5.0 | 0.529 | 0.15884361609772066 |
| CsSnI3 | uniaxial_c | 7.5 | 0.742 | 0.14776317959407206 |
| CsSnI3 | uniaxial_c | 10.0 | 0.9550000000000001 | 0.132874516720664 |
| CsSnI3 | uniaxial_c | 12.5 | 0.9550000000000001 | 0.12208986444418717 |
| CsSnI3 | uniaxial_c | 15.0 | 0.9550000000000001 | 0.10905554731420135 |
| CsSnI3 | uniaxial_c | 17.5 | 1.088 | 0.09701466332467502 |
| CsSnI3 | uniaxial_c | 20.0 | 1.1435 | 0.10496782218256229 |
| CsSnI3 | uniaxial_c | 22.5 | 1.1435 | 0.10672520716189791 |
| CsSnI3 | uniaxial_c | 25.0 | 1.1435 | 0.10786475327928023 |
| CsSnI3 | isotropic | -25.0 | -0.00040133177264478376 | 0.20558043096834155 |
| CsSnI3 | isotropic | -22.5 | 0.3462705550215352 | 0.16903938610000502 |
| CsSnI3 | isotropic | -20.0 | 0.8924838856098627 | 0.1610919366863713 |

Continued on next page

Table S4: Winner-model predictions on the tabulated strain grid. For each material and loading mode we report the strain $\varepsilon$ (%), predictive mean $\mu$ (eV), and predictive uncertainty $\sigma$ (eV). (Continued)

| material | strain_type | $\varepsilon$ (%) | $\mu$ (eV) | $\sigma$ (eV) |
|---|---|---|---|---|
| CsSnI3 | isotropic | -17.5 | 1.3452211157828078 | 0.17643188517090874 |
| CsSnI3 | isotropic | -15.0 | 1.4804347096164865 | 0.16358529827107768 |
| CsSnI3 | isotropic | -12.5 | 1.3112381961801305 | 0.11893072907949975 |
| CsSnI3 | isotropic | -10.0 | 1.0000638176177727 | 0.08082614069120461 |
| CsSnI3 | isotropic | -7.5 | 0.6769059936660344 | 0.06354730966415274 |
| CsSnI3 | isotropic | -5.0 | 0.41349168463678615 | 0.0505694114296324 |
| CsSnI3 | isotropic | -2.5 | 0.30489585880042097 | 0.04255762046425585 |
| CsSnI3 | isotropic | 0.0 | 0.43926482228189845 | 0.04277711457793062 |
| CsSnI3 | isotropic | 2.5 | 0.7783683220236833 | 0.05628878506937339 |
| CsSnI3 | isotropic | 5.0 | 1.1707543520430452 | 0.08577416673273121 |
| CsSnI3 | isotropic | 7.5 | 1.5073563476681373 | 0.1236250566231989 |
| CsSnI3 | isotropic | 10.0 | 1.7913438860363047 | 0.18096263988371541 |
| CsSnI3 | isotropic | 12.5 | 2.0461695847074504 | 0.25809501526061523 |
| CsSnI3 | isotropic | 15.0 | 2.241883777475565 | 0.32351788640913487 |
| CsSnI3 | isotropic | 17.5 | 2.351105015257879 | 0.35910774837538656 |
| CsSnI3 | isotropic | 20.0 | 2.413388722011753 | 0.40765606634541895 |
| CsSnI3 | isotropic | 22.5 | 2.4844410884661916 | 0.521512479129979 |
| CsSnI3 | isotropic | 25.0 | 2.5405742195332124 | 0.6619297373002657 |

Table S5: Lattice and density response versus strain for each material and loading mode. Columns: $a, b, c$ (Å), $c/c_0$, $c/a$, cell volume $V$ (Å$^3$), $V/V_0$, density $\rho$ ($\mathrm{g\,cm^{-3}}$), and $\rho/\rho_0$ as functions of $\varepsilon$ (%).

| material | strain_type | $\varepsilon$ (%) | $a$ (Å) | $b$ (Å) | $c$ (Å) | $c/c_0$ | $V$ (Å$^3$) | $c/a$ | $V/V_0$ | $\rho$ ($\mathrm{g\,cm^{-3}}$) | $\rho/\rho_0$ |
|---|---|---|---|---|---|---|---|---|---|---|---|
| CsSnCl3 | isotropic | -25 | 4.2106 | 4.2106 | 4.2106 | 1.3333 | 74.6479 | 1 | 2.3704 | 31.0244 | 0.1083 |
| CsSnCl3 | isotropic | -20 | 4.4913 | 4.4913 | 4.4913 | 1.25 | 90.5949 | 1 | 1.9531 | 25.5633 | 0.1314 |
| CsSnCl3 | isotropic | -15 | 4.772 | 4.772 | 4.772 | 1.1765 | 108.6653 | 1 | 1.6283 | 5.4703 | 0.6141 |
| CsSnCl3 | isotropic | -10 | 5.0527 | 5.0527 | 5.0527 | 1.1111 | 128.9916 | 1 | 1.3717 | 4.6083 | 0.729 |
| CsSnCl3 | isotropic | -5 | 5.3334 | 5.3334 | 5.3334 | 1.0526 | 151.7067 | 1 | 1.1664 | 3.9183 | 0.8573 |
| CsSnCl3 | isotropic | 0 | 5.6141 | 5.6141 | 5.6141 | 1 | 176.9432 | 1 | 1 | 3.3593 | 1 |
| CsSnCl3 | isotropic | 5 | 5.8948 | 5.8948 | 5.8948 | 0.9524 | 204.8339 | 1 | 0.8638 | 2.902 | 1.1576 |
| CsSnCl3 | isotropic | 10 | 6.1755 | 6.1755 | 6.1755 | 0.9091 | 235.5114 | 1 | 0.7513 | 2.524 | 1.3309 |
| CsSnCl3 | isotropic | 15 | 6.4562 | 6.4562 | 6.4562 | 0.8696 | 269.1085 | 1 | 0.6575 | 2.2089 | 1.5208 |
| CsSnCl3 | isotropic | 20 | 6.7369 | 6.7369 | 6.7369 | 0.8333 | 305.7579 | 1 | 0.5787 | 1.9441 | 1.7279 |
| CsSnCl3 | isotropic | 25 | 7.0176 | 7.0176 | 7.0176 | 0.8 | 345.5922 | 1 | 0.512 | 1.72 | 1.953 |
| CsSnCl3 | uniaxial c | -25 | 5.6141 | 5.6141 | 4.2106 | 1.3333 | 132.7074 | 0.75 | 1.3333 | 4.4792 | 0.75 |
| CsSnCl3 | uniaxial c | -20 | 5.6141 | 5.6141 | 4.4913 | 1.25 | 141.5546 | 0.8 | 1.25 | 4.1993 | 0.8 |

Continued on next page

Table S5: Lattice and density response versus strain for each material and loading mode. Columns: $a, b, c$ (Å), $c/c_0$, $c/a$, cell volume $V$ (Å$^3$), $V/V_0$, density $\rho$ (g cm$^{-3}$), and $\rho/\rho_0$ as functions of $\varepsilon$ (%). (Continued)

| material | strain_type | $\varepsilon$ (%) | $a$ (Å) | $b$ (Å) | $c$ (Å) | $c/c_0$ | $V$ (Å$^3$) | $c/a$ | $V/V_0$ | $\rho$ (g cm$^{-3}$) | $\rho/\rho_0$ |
|---|---|---|---|---|---|---|---|---|---|---|---|
| CsSnCl3 | uniaxial c | -15 | 5.6141 | 5.6141 | 4.772 | 1.1765 | 150.4017 | 0.85 | 1.1765 | 3.9523 | 0.85 |
| CsSnCl3 | uniaxial c | -10 | 5.6141 | 5.6141 | 5.0527 | 1.1111 | 159.2489 | 0.9 | 1.1111 | 3.7327 | 0.9 |
| CsSnCl3 | uniaxial c | -5 | 5.6141 | 5.6141 | 5.3334 | 1.0526 | 168.096 | 0.95 | 1.0526 | 3.5362 | 0.9499 |
| CsSnCl3 | uniaxial c | 0 | 5.6141 | 5.6141 | 5.6141 | 1 | 176.9432 | 1 | 1 | 3.3593 | 1 |
| CsSnCl3 | uniaxial c | 5 | 5.6141 | 5.6141 | 5.8948 | 0.9524 | 185.7904 | 1.05 | 0.9524 | 3.1995 | 1.0499 |
| CsSnCl3 | uniaxial c | 10 | 5.6141 | 5.6141 | 6.1755 | 0.9091 | 194.6375 | 1.1 | 0.9091 | 3.054 | 1.0999 |
| CsSnCl3 | uniaxial c | 15 | 5.6141 | 5.6141 | 6.4562 | 0.8696 | 203.4847 | 1.15 | 0.8696 | 2.9212 | 1.1499 |
| CsSnCl3 | uniaxial c | 20 | 5.6141 | 5.6141 | 6.7369 | 0.8333 | 212.3318 | 1.2 | 0.8333 | 2.7995 | 1.1999 |
| CsSnCl3 | uniaxial c | 25 | 5.6141 | 5.6141 | 7.0176 | 0.8 | 221.179 | 1.25 | 0.8 | 2.6875 | 1.2499 |
| CsSnBr3 | isotropic | -25 | 4.4115 | 4.4115 | 4.4115 | 1.2726 | 85.8535 | 1 | 2.3704 | 9.503 | 0.4219 |
| CsSnBr3 | isotropic | -20 | 4.7056 | 4.7056 | 4.7056 | 1.1931 | 104.1943 | 1 | 1.9531 | 7.8303 | 0.512 |
| CsSnBr3 | isotropic | -15 | 4.9997 | 4.9997 | 4.9997 | 1.1229 | 124.9772 | 1 | 1.6283 | 6.5281 | 0.6141 |
| CsSnBr3 | isotropic | -10 | 5.2938 | 5.2938 | 5.2938 | 1.0605 | 148.3548 | 1 | 1.3717 | 5.4994 | 0.729 |
| CsSnBr3 | isotropic | -5 | 5.5879 | 5.5879 | 5.5879 | 1.0047 | 174.4797 | 1 | 1.1664 | 4.676 | 0.8573 |
| CsSnBr3 | isotropic | 0 | 5.882 | 5.882 | 5.882 | 0.9545 | 203.5046 | 1 | 1 | 4.0089 | 1 |
| CsSnBr3 | isotropic | 5 | 6.1761 | 6.1761 | 6.1761 | 0.909 | 235.582 | 1 | 0.8638 | 3.4632 | 1.1576 |
| CsSnBr3 | isotropic | 10 | 6.4702 | 6.4702 | 6.4702 | 0.8677 | 270.8646 | 1 | 0.7513 | 3.0121 | 1.3309 |
| CsSnBr3 | isotropic | 15 | 6.7643 | 6.7643 | 6.7643 | 0.83 | 309.505 | 1 | 0.6575 | 2.636 | 1.5208 |
| CsSnBr3 | isotropic | 20 | 7.0584 | 7.0584 | 7.0584 | 0.7954 | 351.6559 | 1 | 0.5787 | 2.3201 | 1.7279 |
| CsSnBr3 | isotropic | 25 | 7.3525 | 7.3525 | 7.3525 | 0.7636 | 397.4699 | 1 | 0.512 | 2.0527 | 1.953 |
| CsSnBr3 | uniaxial c | -25 | 5.882 | 5.882 | 4.4115 | 1.2726 | 152.6284 | 0.75 | 1.3333 | 5.3455 | 0.75 |
| CsSnBr3 | uniaxial c | -20 | 5.882 | 5.882 | 4.7056 | 1.1931 | 162.8037 | 0.8 | 1.25 | 5.0114 | 0.8 |
| CsSnBr3 | uniaxial c | -15 | 5.882 | 5.882 | 4.9997 | 1.1229 | 172.9789 | 0.85 | 1.1765 | 4.7166 | 0.85 |
| CsSnBr3 | uniaxial c | -10 | 5.882 | 5.882 | 5.2938 | 1.0605 | 183.1541 | 0.9 | 1.1111 | 4.4545 | 0.9 |
| CsSnBr3 | uniaxial c | -5 | 5.882 | 5.882 | 5.5879 | 1.0047 | 193.3293 | 0.95 | 1.0526 | 4.2201 | 0.95 |
| CsSnBr3 | uniaxial c | 0 | 5.882 | 5.882 | 5.882 | 0.9545 | 203.5046 | 1 | 1 | 4.0089 | 1 |
| CsSnBr3 | uniaxial c | 5 | 5.882 | 5.882 | 6.1761 | 0.909 | 213.6798 | 1.05 | 0.9524 | 3.8182 | 1.05 |
| CsSnBr3 | uniaxial c | 10 | 5.882 | 5.882 | 6.4702 | 0.8677 | 223.855 | 1.1 | 0.9091 | 3.6446 | 1.1 |
| CsSnBr3 | uniaxial c | 15 | 5.882 | 5.882 | 6.7643 | 0.83 | 234.0303 | 1.15 | 0.8696 | 3.4862 | 1.15 |
| CsSnBr3 | uniaxial c | 20 | 5.882 | 5.882 | 7.0584 | 0.7954 | 244.2055 | 1.2 | 0.8333 | 3.3409 | 1.2 |
| CsSnBr3 | uniaxial c | 25 | 5.882 | 5.882 | 7.3525 | 0.7636 | 254.3807 | 1.25 | 0.8 | 3.2073 | 1.2499 |
| CsSnI3 | isotropic | -25 | 4.7053 | 4.7053 | 4.7053 | 1.1931 | 104.1729 | 1 | 2.3704 | 10.0795 | 0.4219 |
| CsSnI3 | isotropic | -20 | 5.019 | 5.019 | 5.019 | 1.1186 | 126.4273 | 1 | 1.9531 | 8.3052 | 0.512 |
| CsSnI3 | isotropic | -15 | 5.3326 | 5.3326 | 5.3326 | 1.0528 | 151.6448 | 1 | 1.6283 | 6.9241 | 0.6141 |
| CsSnI3 | isotropic | -10 | 5.6463 | 5.6463 | 5.6463 | 0.9943 | 180.0107 | 1 | 1.3717 | 5.833 | 0.729 |
| CsSnI3 | isotropic | -5 | 5.96 | 5.96 | 5.96 | 0.942 | 211.7101 | 1 | 1.1664 | 4.9596 | 0.8573 |

Continued on next page

Table S5: Lattice and density response versus strain for each material and loading mode. Columns: $a, b, c$ (Å), $c/c_0$, $c/a$, cell volume $V$ (Å$^3$), $V/V_0$, density $\rho$ ($\mathrm{g\,cm^{-3}}$), and $\rho/\rho_0$ as functions of $\varepsilon$ (%). (Continued)

| material | strain_type | $\varepsilon$ (%) | $a$ (Å) | $b$ (Å) | $c$ (Å) | $c/c_0$ | $V$ (Å$^3$) | $c/a$ | $V/V_0$ | $\rho$ ($\mathrm{g\,cm^{-3}}$) | $\rho/\rho_0$ |
|---|---|---|---|---|---|---|---|---|---|---|---|
| CsSnI3 | isotropic | 0 | 6.2737 | 6.2737 | 6.2737 | 0.8949 | 246.9282 | 1 | 1 | 4.2521 | 1 |
| CsSnI3 | isotropic | 5 | 6.5874 | 6.5874 | 6.5874 | 0.8522 | 285.8503 | 1 | 0.8638 | 3.6733 | 1.1576 |
| CsSnI3 | isotropic | 10 | 6.9011 | 6.9011 | 6.9011 | 0.8135 | 328.6615 | 1 | 0.7513 | 3.1948 | 1.331 |
| CsSnI3 | isotropic | 15 | 7.2148 | 7.2148 | 7.2148 | 0.7781 | 375.547 | 1 | 0.6575 | 2.7959 | 1.5208 |
| CsSnI3 | isotropic | 20 | 7.5284 | 7.5284 | 7.5284 | 0.7457 | 426.6921 | 1 | 0.5787 | 2.4608 | 1.7279 |
| CsSnI3 | isotropic | 25 | 7.8421 | 7.8421 | 7.8421 | 0.7159 | 482.2818 | 1 | 0.512 | 2.1772 | 1.9531 |
| CsSnI3 | uniaxial c | -25 | 6.2737 | 6.2737 | 4.7053 | 1.1931 | 185.1962 | 0.75 | 1.3333 | 5.6697 | 0.75 |
| CsSnI3 | uniaxial c | -20 | 6.2737 | 6.2737 | 5.019 | 1.1186 | 197.5426 | 0.8 | 1.25 | 5.3153 | 0.8 |
| CsSnI3 | uniaxial c | -15 | 6.2737 | 6.2737 | 5.3326 | 1.0528 | 209.889 | 0.85 | 1.1765 | 5.0027 | 0.85 |
| CsSnI3 | uniaxial c | -10 | 6.2737 | 6.2737 | 5.6463 | 0.9943 | 222.2354 | 0.9 | 1.1111 | 4.7248 | 0.9 |
| CsSnI3 | uniaxial c | -5 | 6.2737 | 6.2737 | 5.96 | 0.942 | 234.5818 | 0.95 | 1.0526 | 4.4761 | 0.95 |
| CsSnI3 | uniaxial c | 0 | 6.2737 | 6.2737 | 6.2737 | 0.8949 | 246.9282 | 1 | 1 | 4.2521 | 1 |
| CsSnI3 | uniaxial c | 5 | 6.2737 | 6.2737 | 6.5874 | 0.8522 | 259.2747 | 1.05 | 0.9524 | 4.0498 | 1.05 |
| CsSnI3 | uniaxial c | 10 | 6.2737 | 6.2737 | 6.9011 | 0.8135 | 271.6211 | 1.1 | 0.9091 | 3.8657 | 1.1 |
| CsSnI3 | uniaxial c | 15 | 6.2737 | 6.2737 | 7.2148 | 0.7781 | 283.9675 | 1.15 | 0.8696 | 3.6976 | 1.15 |
| CsSnI3 | uniaxial c | 20 | 6.2737 | 6.2737 | 7.5284 | 0.7457 | 296.3139 | 1.2 | 0.8333 | 3.5436 | 1.2 |
| CsSnI3 | uniaxial c | 25 | 6.2737 | 6.2737 | 7.8421 | 0.7159 | 308.6603 | 1.25 | 0.8 | 3.4018 | 1.25 |

Table S6: Small-strain $CsSnBr_3$ band-gap comparison (ours isotropic vs. El Badraoui *et al.* [1] hydrostatic). $\Delta\,(\%) = \dfrac{E_g^{\text{ours}} - E_g^{[1]}}{E_g^{[1]}} \times 100$.

| Strain (%) | Our ML $E_g$ (eV) | El Badraoui *et al.* [1] $E_g$ (eV) | $\Delta$ (eV) | $\Delta$ (%) |
|---|---|---|---|---|
| −3 | 0.372 | 0.604 | −0.232 | −38.4 |
| −2 | 0.425 | 0.841 | −0.416 | −49.5 |
| −1 | 0.506 | 1.062 | −0.556 | −52.4 |
| 0 | 0.615 | 1.272 | −0.657 | −51.7 |
| +1 | 0.753 | 1.470 | −0.717 | −48.8 |
| +2 | 0.918 | 1.651 | −0.733 | −44.4 |
| +3 | 1.113 | 1.823 | −0.710 | −39.0 |

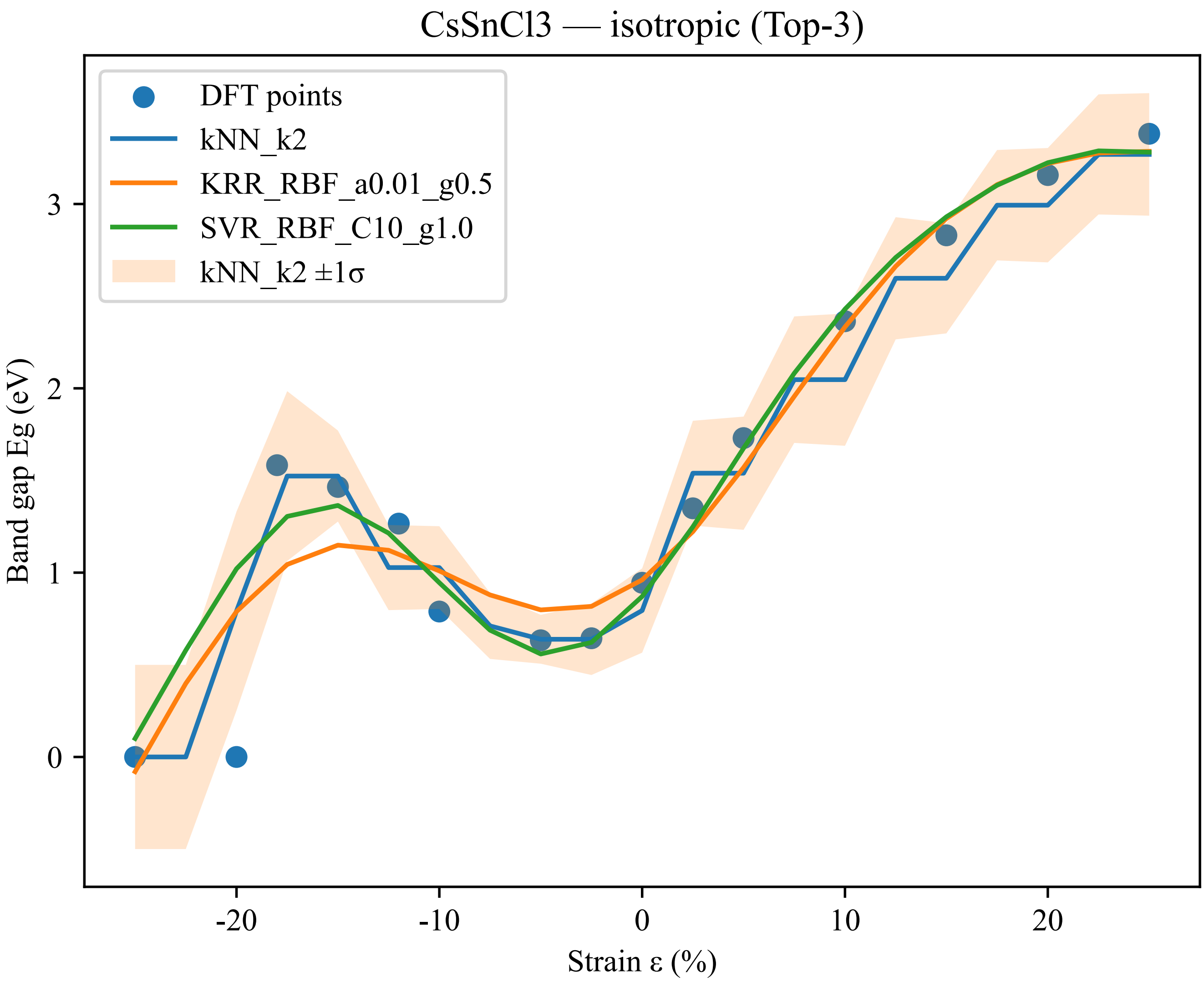


Fig. S1: $CsSnCl_3$ — isotropic strain. Top-3 surrogate models versus DFT band gaps; the winner is shown as a solid curve with its $\pm 1\sigma$ predictive band.

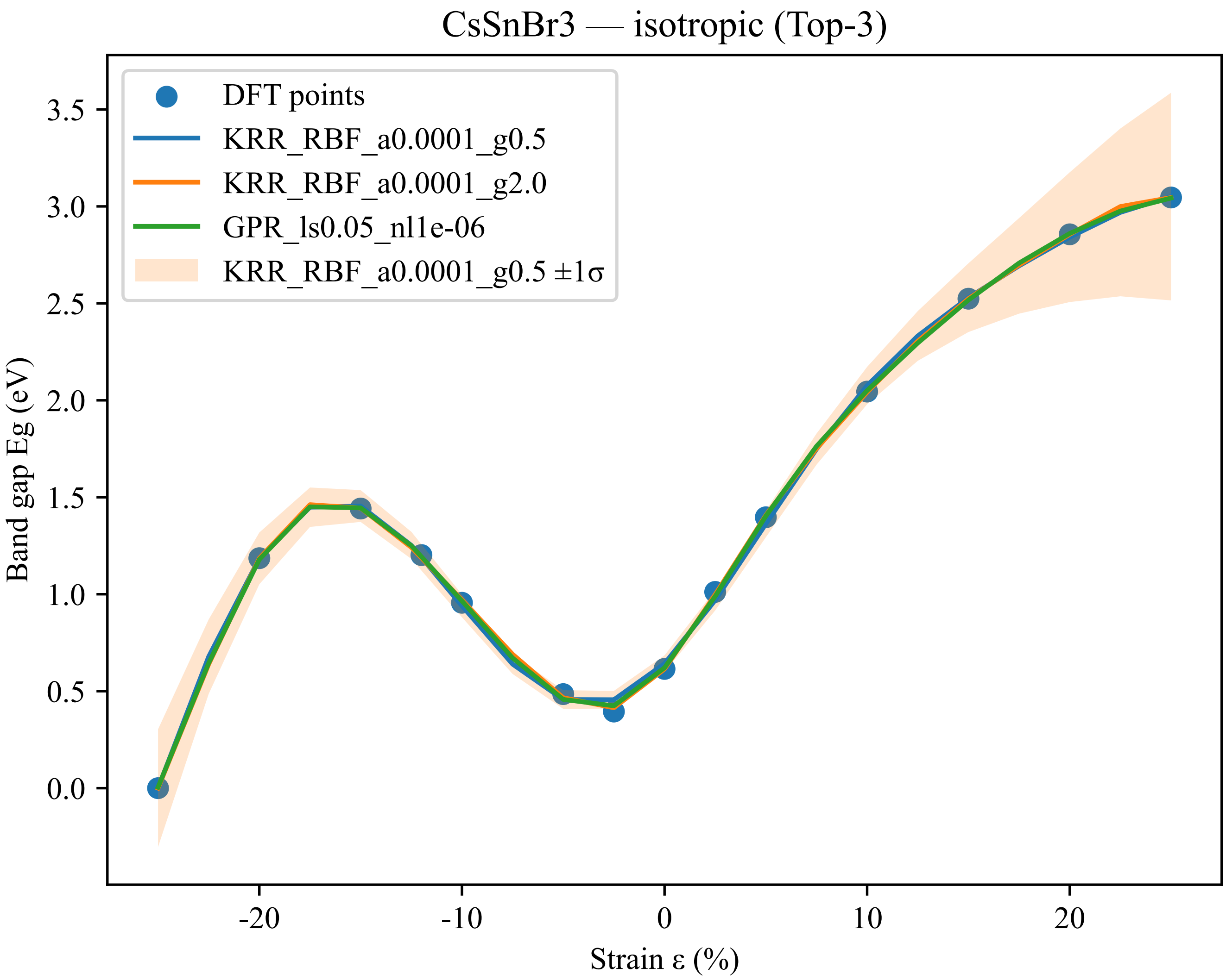


Fig. S2: $CsSnBr_3$ — isotropic strain. Top-3 surrogate models versus DFT band gaps; the winner is shown with its $\pm 1\sigma$ predictive band.

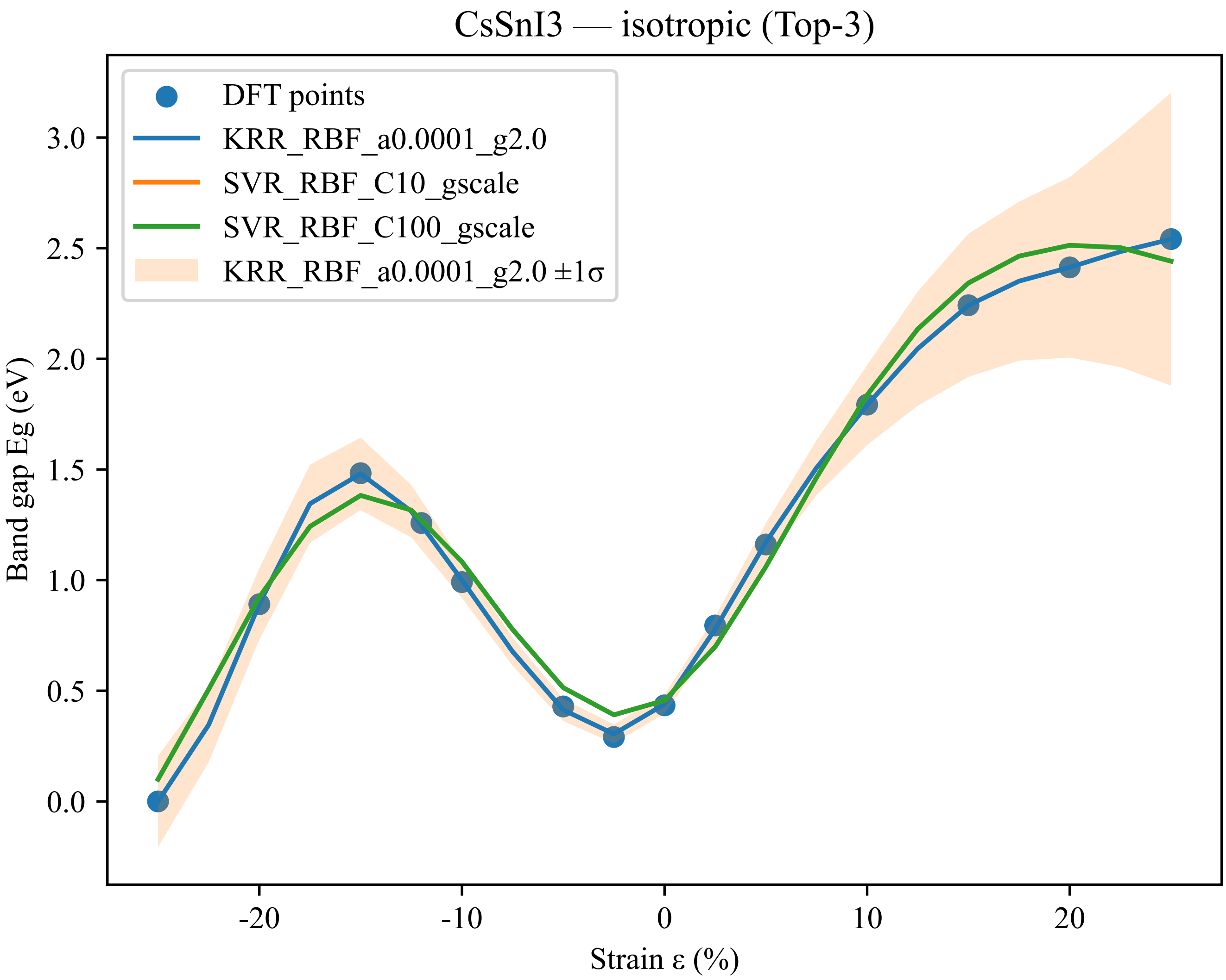


Fig. S3: $CsSnI_3$ — isotropic strain. Top-3 surrogate models versus DFT band gaps; the winner is shown with its $\pm 1\sigma$ predictive band.

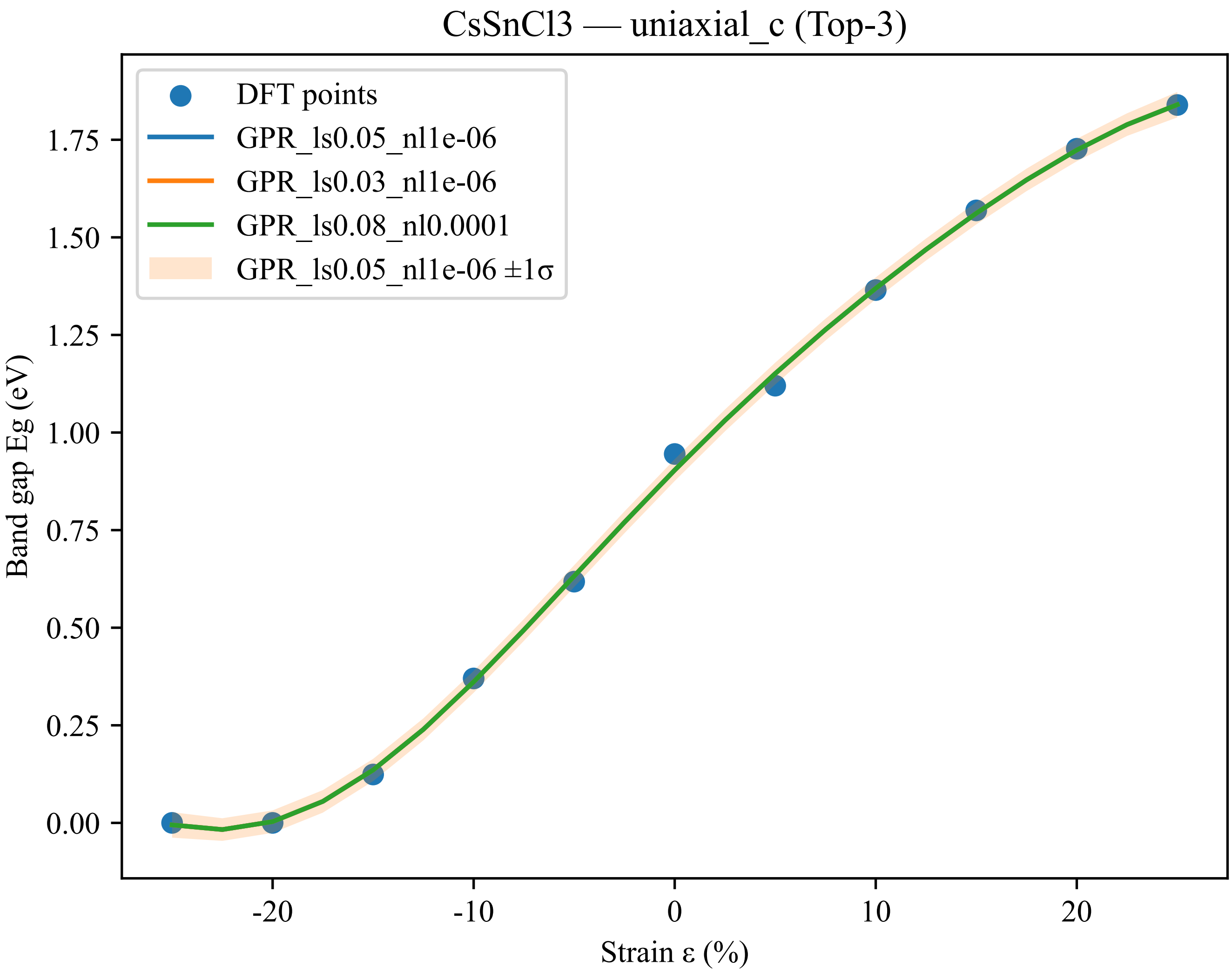


Fig. S4: $CsSnCl_3$ — uniaxial-$c$ strain. Top-3 surrogate models versus DFT band gaps; the winner is shown with its $\pm 1\sigma$ predictive band.

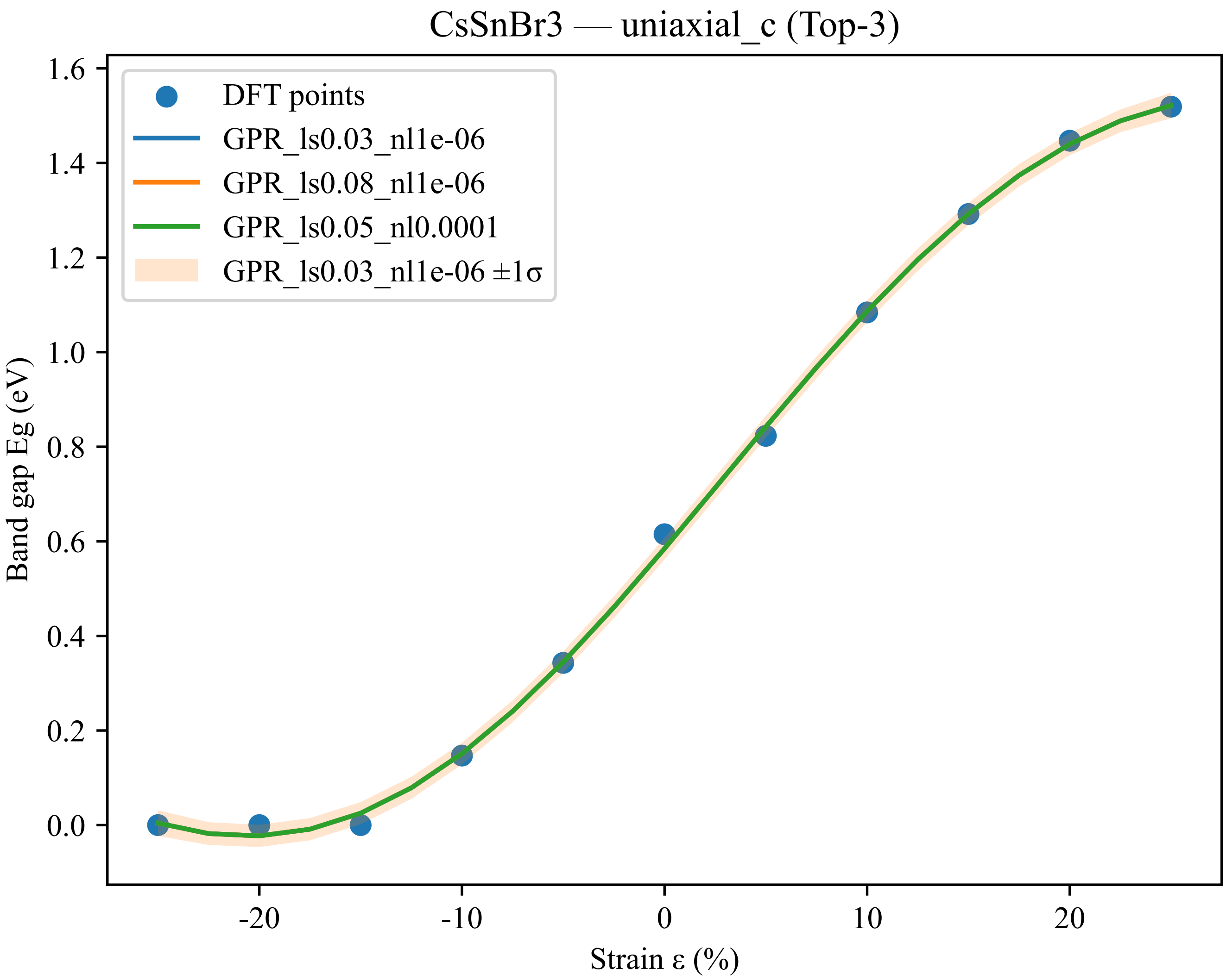


Fig. S5: $CsSnBr_3$ — uniaxial-$c$ strain. Top-3 surrogate models versus DFT band gaps; the winner is shown with its $\pm 1\sigma$ predictive band.

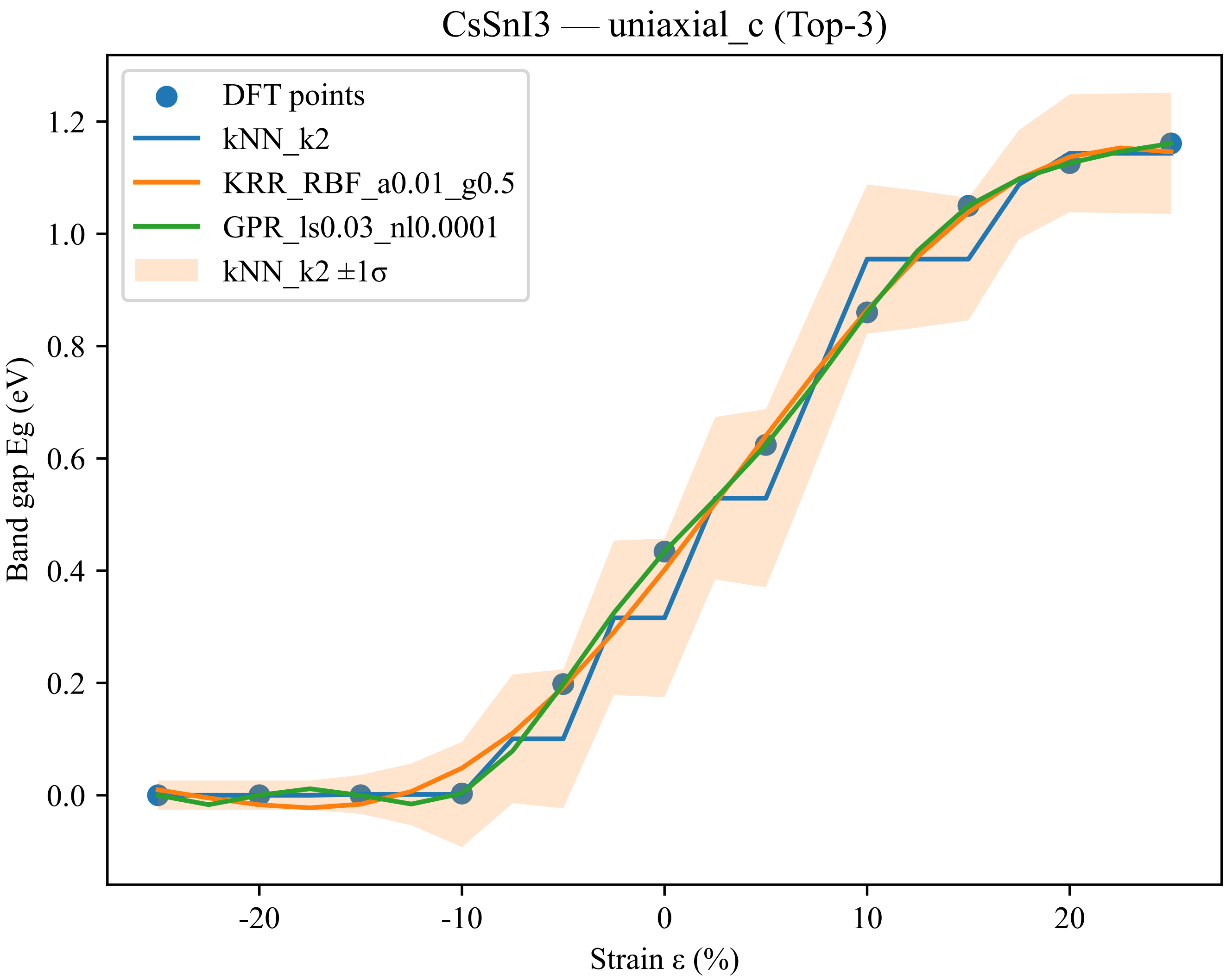


Fig. S6: $CsSnI_3$ — uniaxial-$c$ strain. Top-3 surrogate models versus DFT band gaps; the winner is shown with its $\pm 1\sigma$ predictive band.

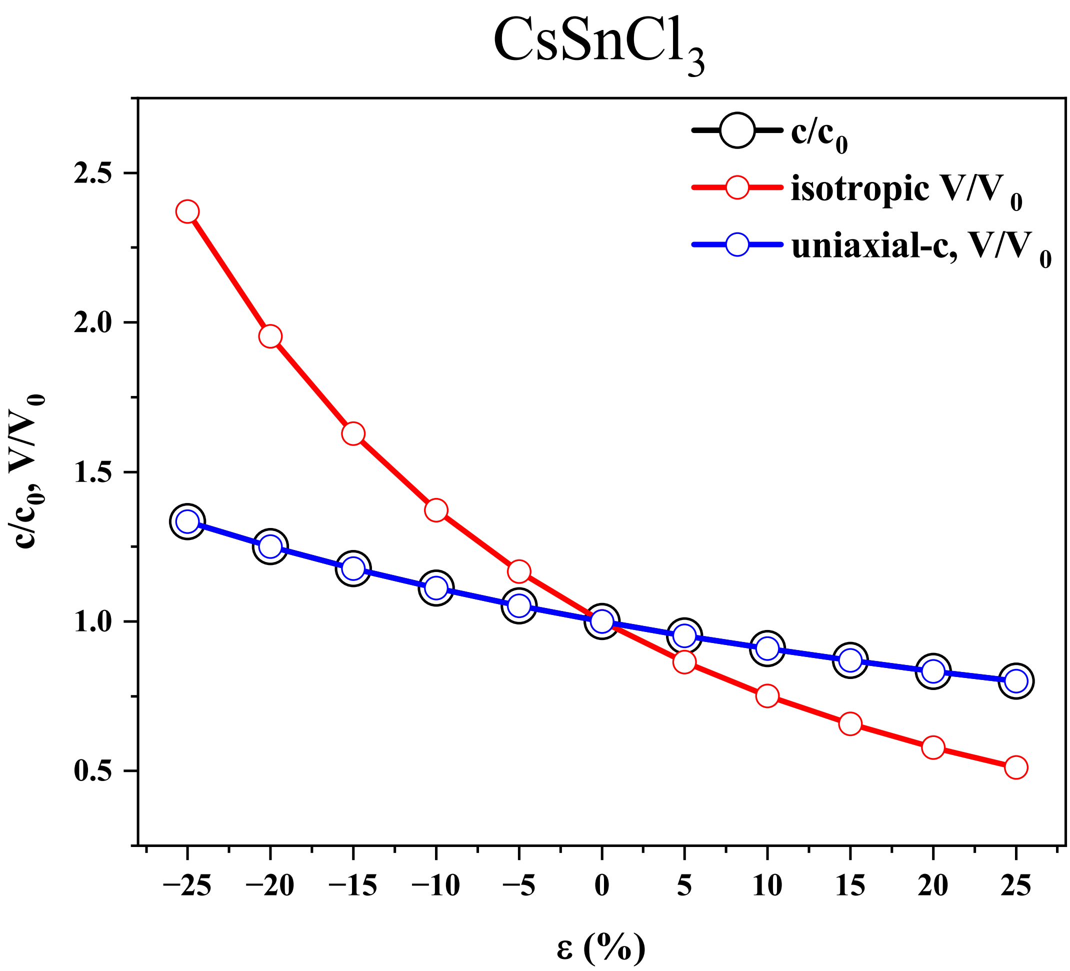


Fig. S7: $CsSnCl_3$: Evolution of $c/c_0$ and $V/V_0$ with strain $\varepsilon$ for isotropic and uniaxial-$c$ loading. Uniaxial-$c$ varies $c$ while holding $a$ and $b$ fixed; isotropic scales all axes equally.

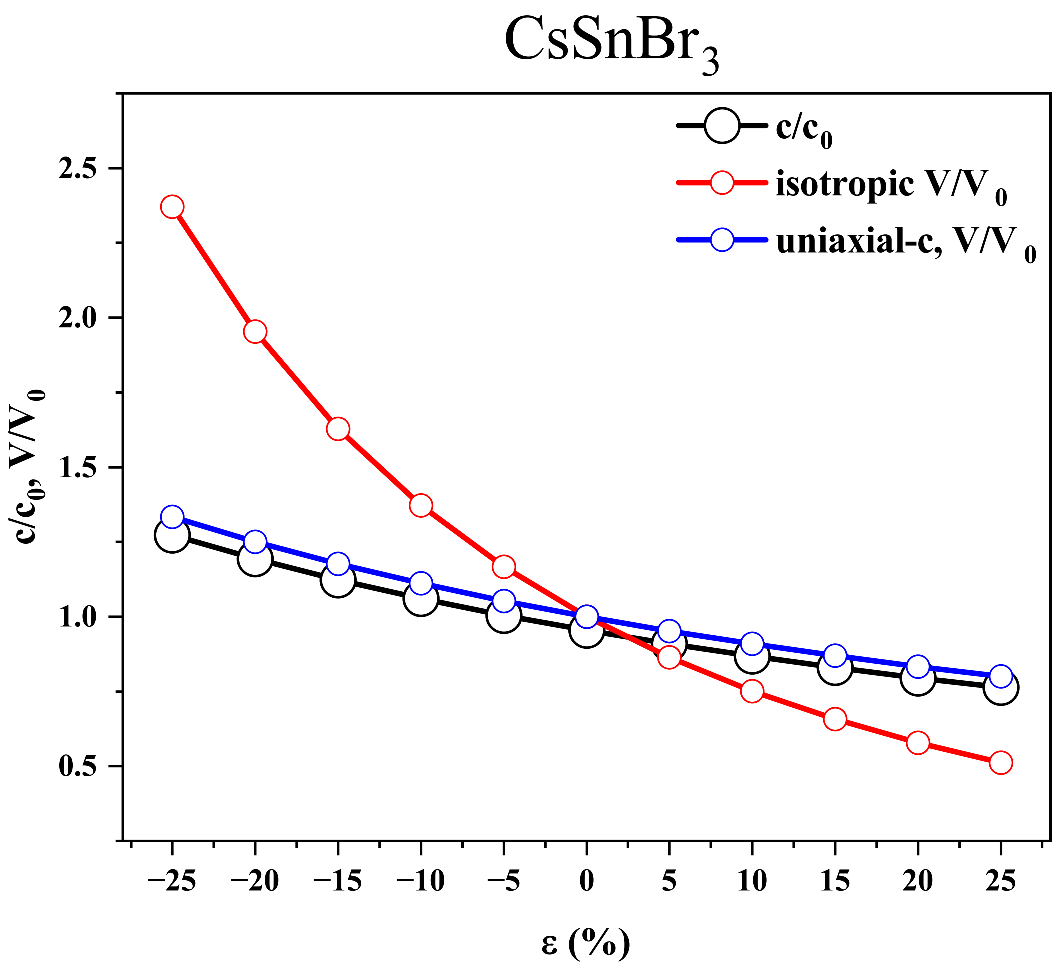


Fig. S8: $CsSnBr_3$: Evolution of $c/c_0$ and $V/V_0$ with strain $\varepsilon$ for isotropic and uniaxial-$c$ loading. Uniaxial-$c$ varies $c$ while holding $a$ and $b$ fixed; isotropic scales all axes equally.

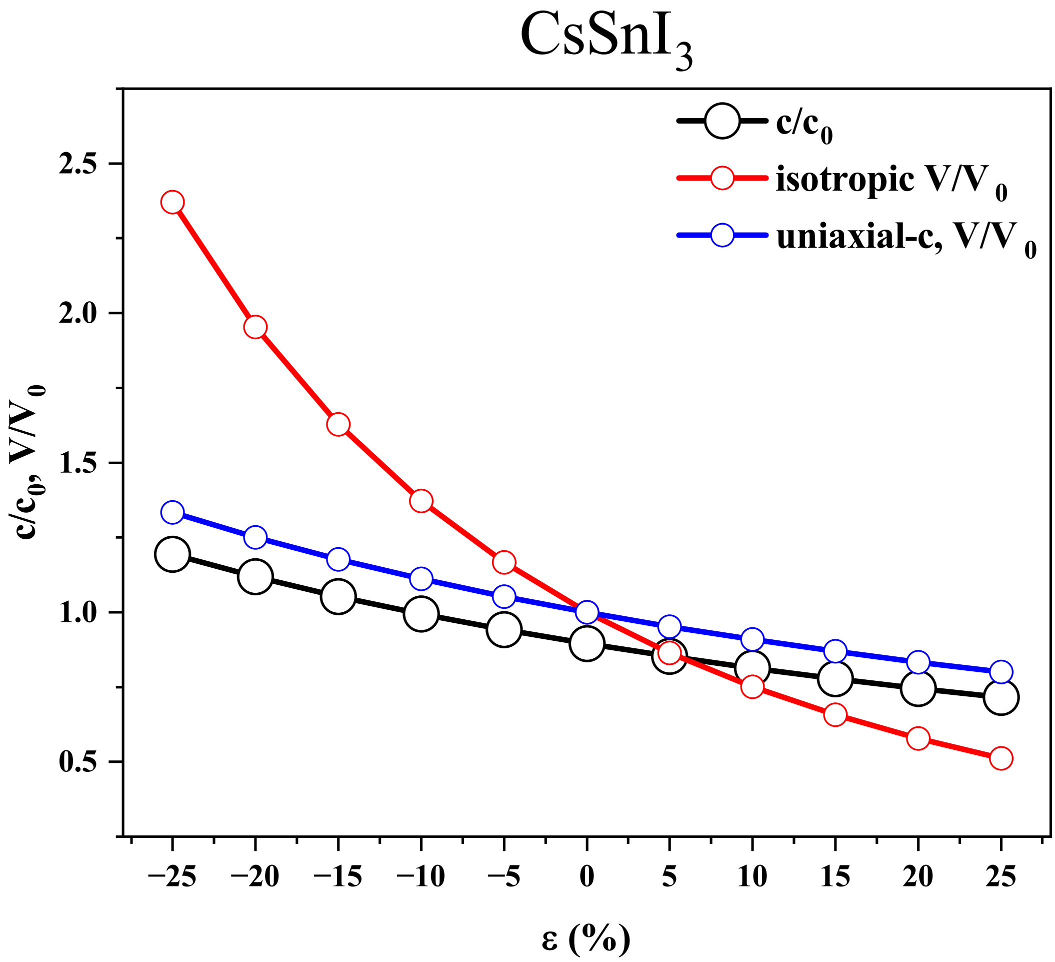


Fig. S9: $CsSnI_3$: Evolution of $c/c_0$ and $V/V_0$ with strain $\varepsilon$ for isotropic and uniaxial-$c$ loading. Uniaxial-$c$ varies $c$ while holding $a$ and $b$ fixed; isotropic scales all axes equally.

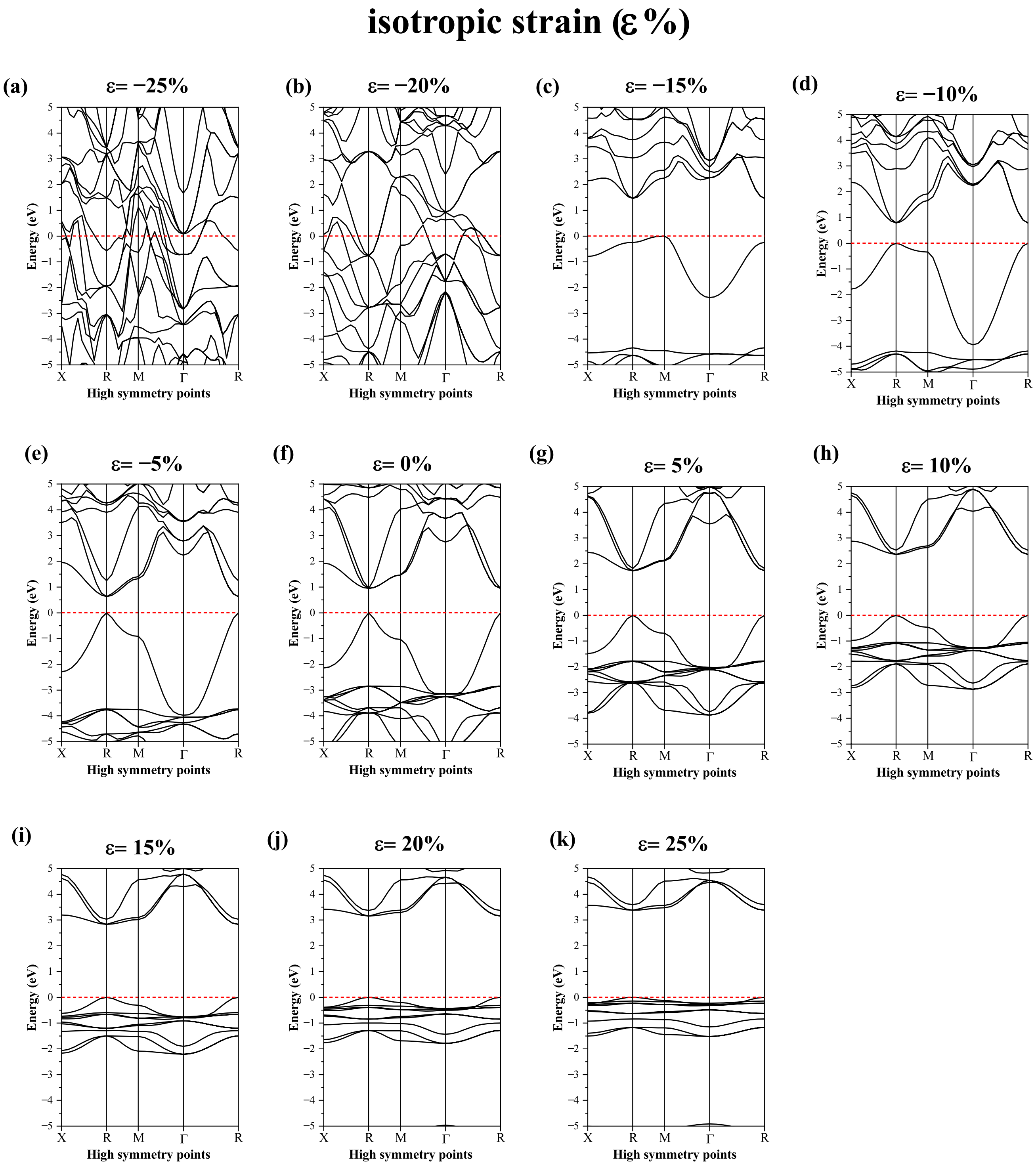


Fig. S10: $CsSnCl_3$ — isotropic: electronic band structures across $\varepsilon = -25\%$ to $+25\%$. Metallization windows ($E_g \approx 0$) and notable band re-orderings are indicated.

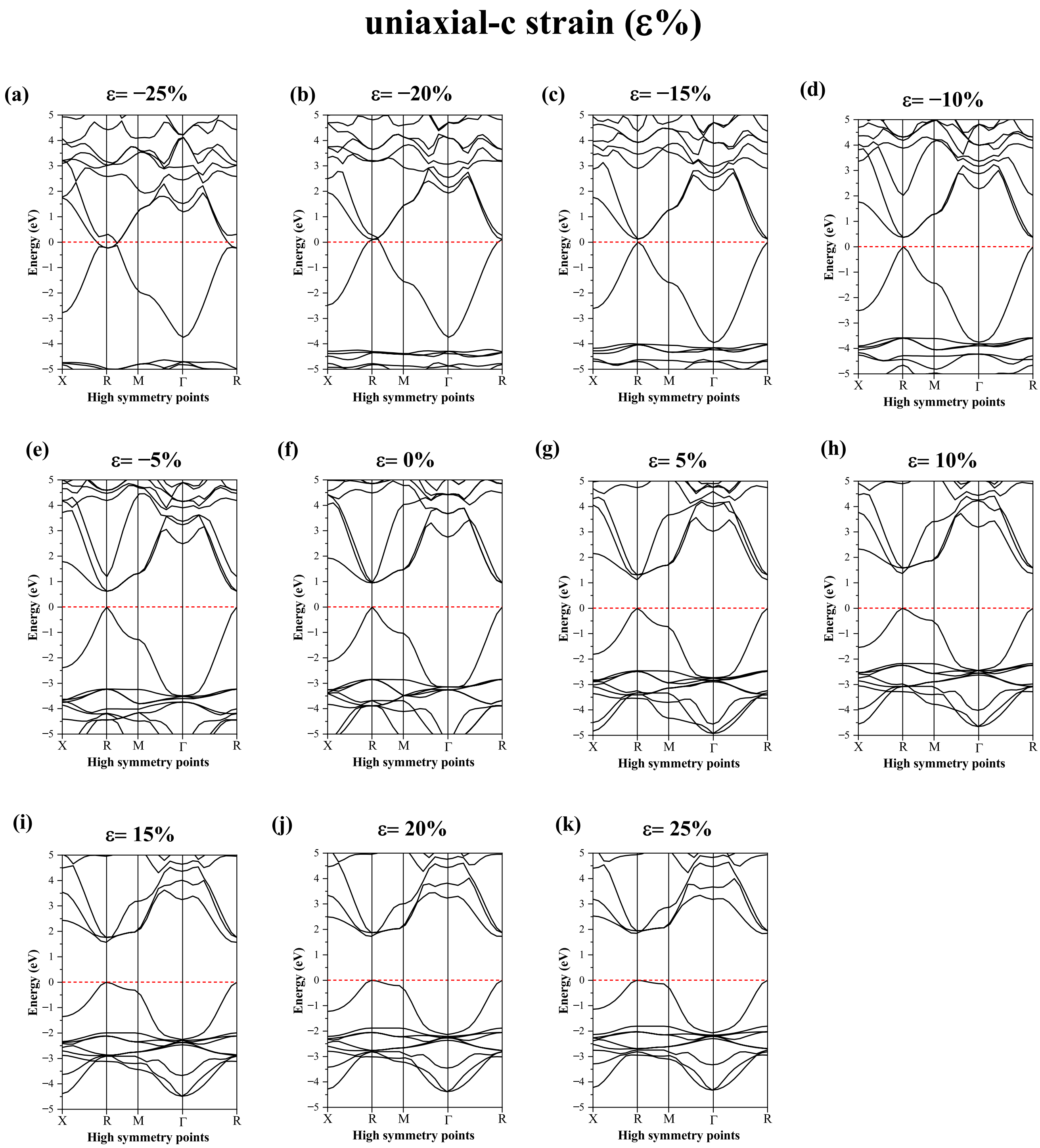


Fig. S11: $CsSnCl_3$ — uniaxial-$c$: electronic band structures across $\varepsilon = -25\%$ to $+25\%$. Metallization windows ($E_g \approx 0$) and notable band re-orderings are indicated.

# isotropic strain (ε %)

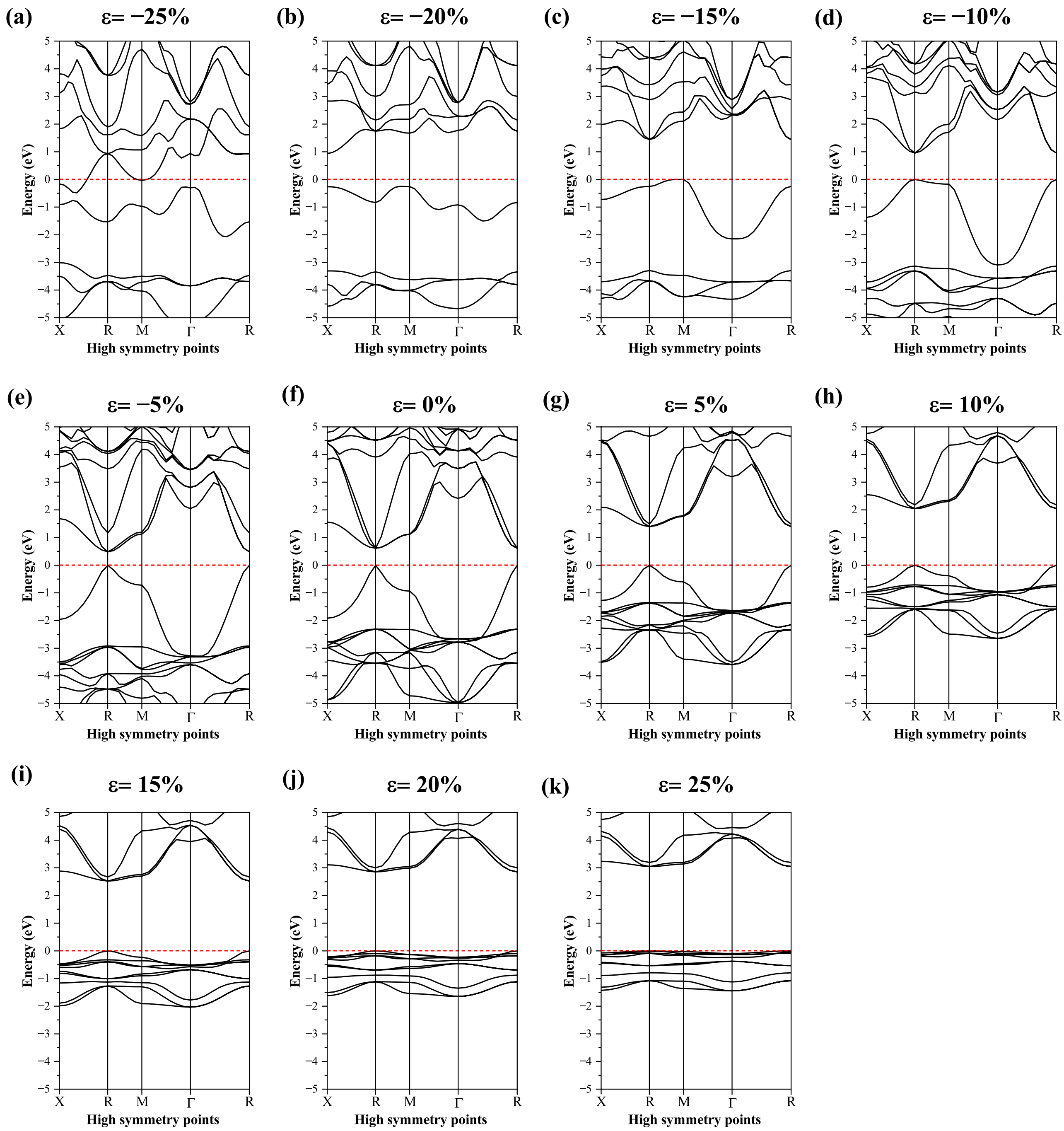


Fig. S12: $CsSnBr_3$ — isotropic: electronic band structures across $\varepsilon = -25\%$ to $+25\%$. Metallization windows ($E_g \approx 0$) and notable band re-orderings are indicated.

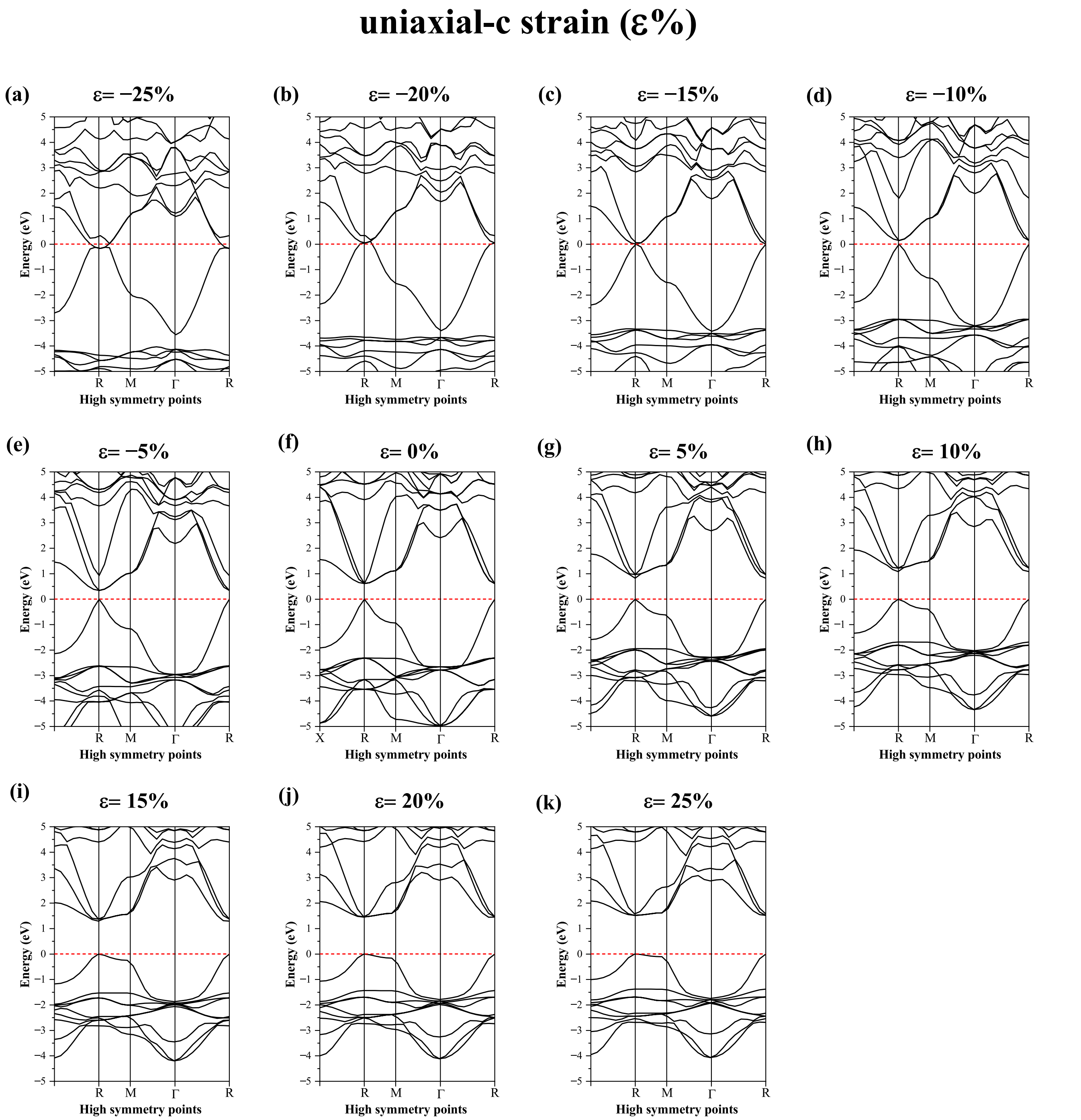


Fig. S13: $CsSnBr_3$ — uniaxial-$c$: electronic band structures across $\varepsilon = -25\%$ to $+25\%$. Metallization windows ($E_g \approx 0$) and notable band re-orderings are indicated.

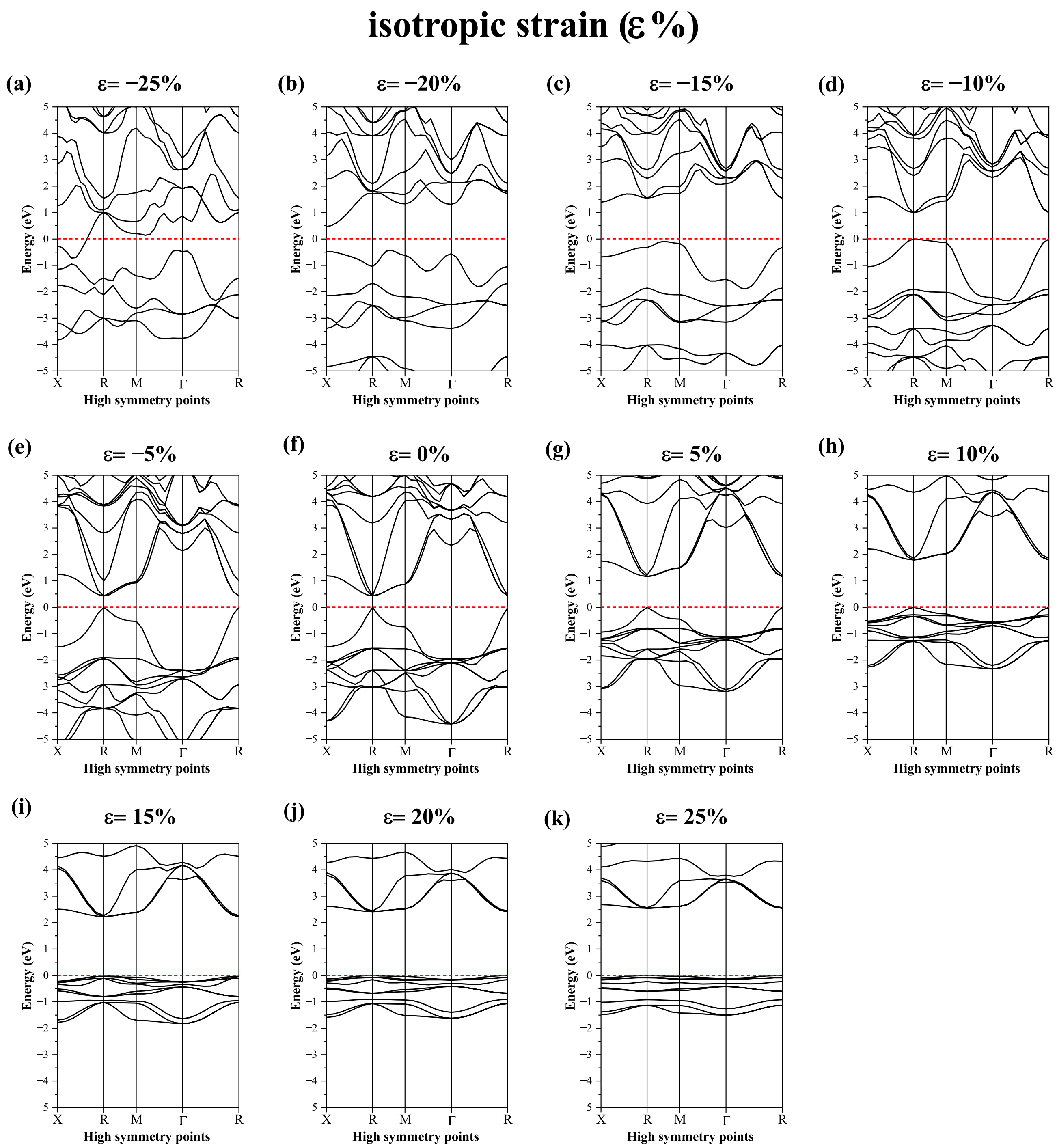


Fig. S14: $CsSnI_3$ — isotropic: electronic band structures across $\varepsilon = -25\%$ to $+25\%$. Metallization windows ($E_g \approx 0$) and notable band re-orderings are indicated.

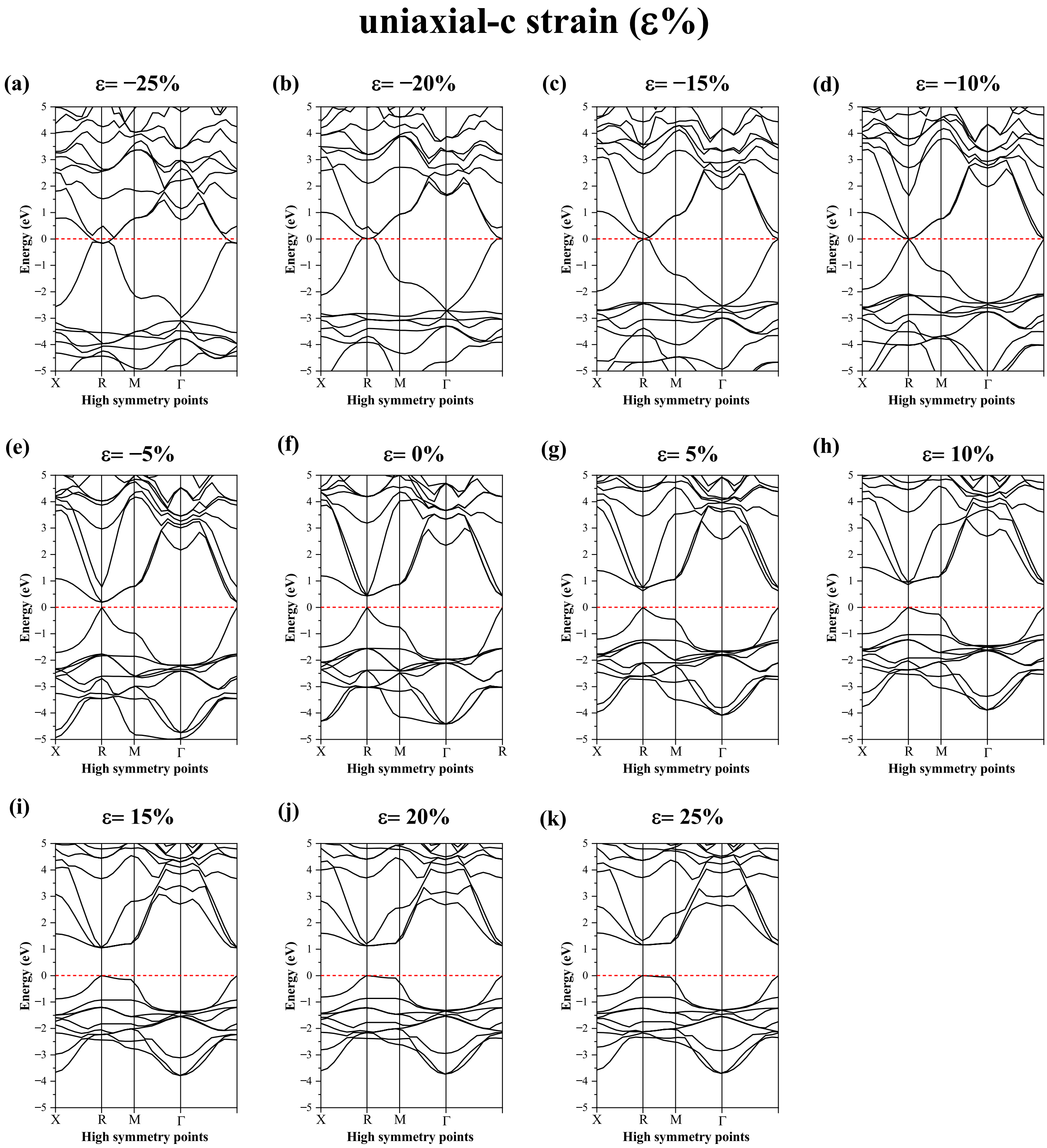


Fig. S15: $CsSnI_3$ — uniaxial-$c$: electronic band structures across $\varepsilon = -25\%$ to $+25\%$. Metallization windows ($E_g \approx 0$) and notable band re-orderings are indicated.

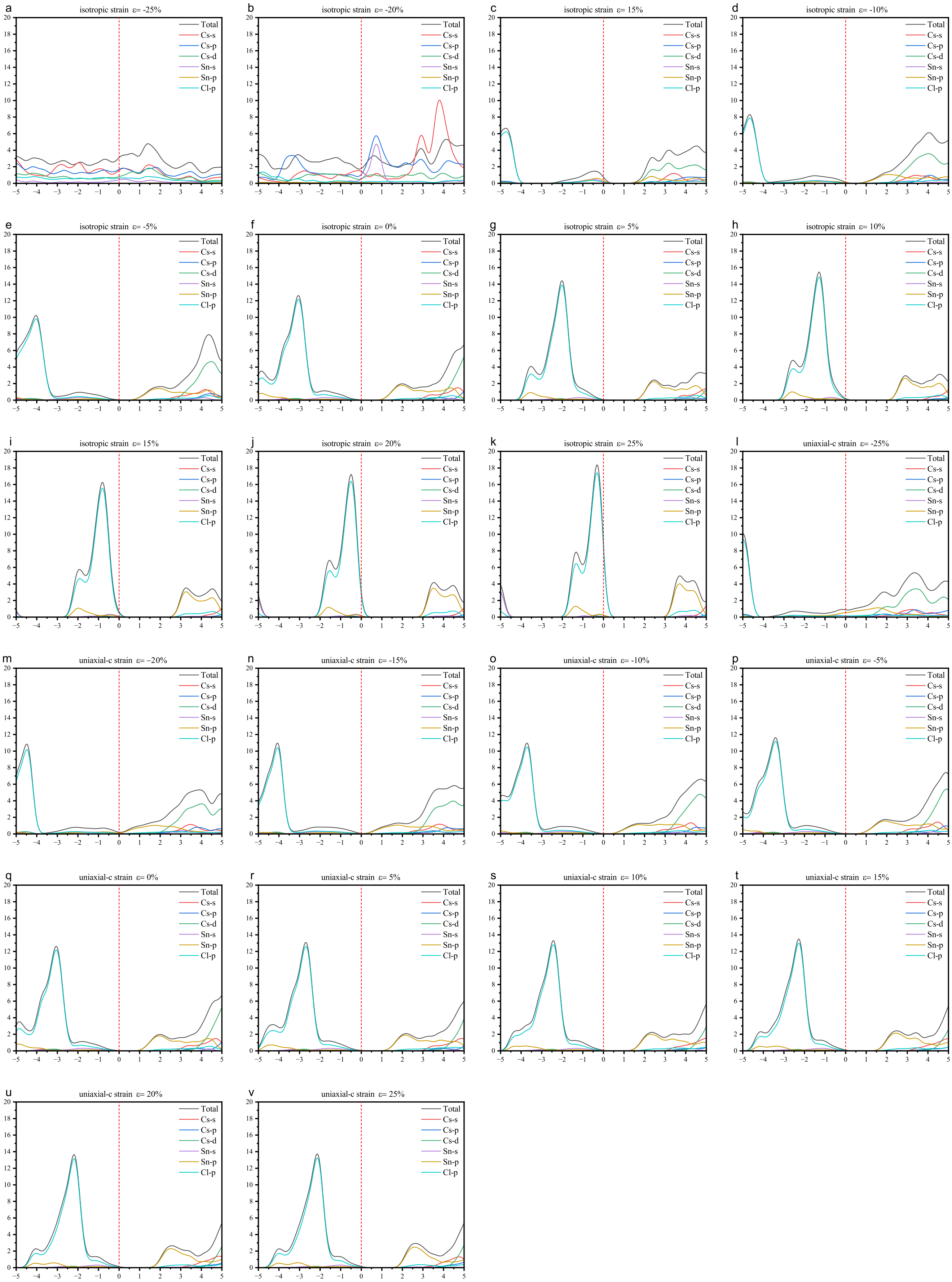


Fig. S16: $CsSnCl_3$: total and projected DOS versus strain $\varepsilon$ for isotropic and uniaxial-$c$ loading. $E_F$ is marked. States near the VBM are mainly Sn-$p$ and X-$p$; the CBM shows notable Sn-$s$ character.

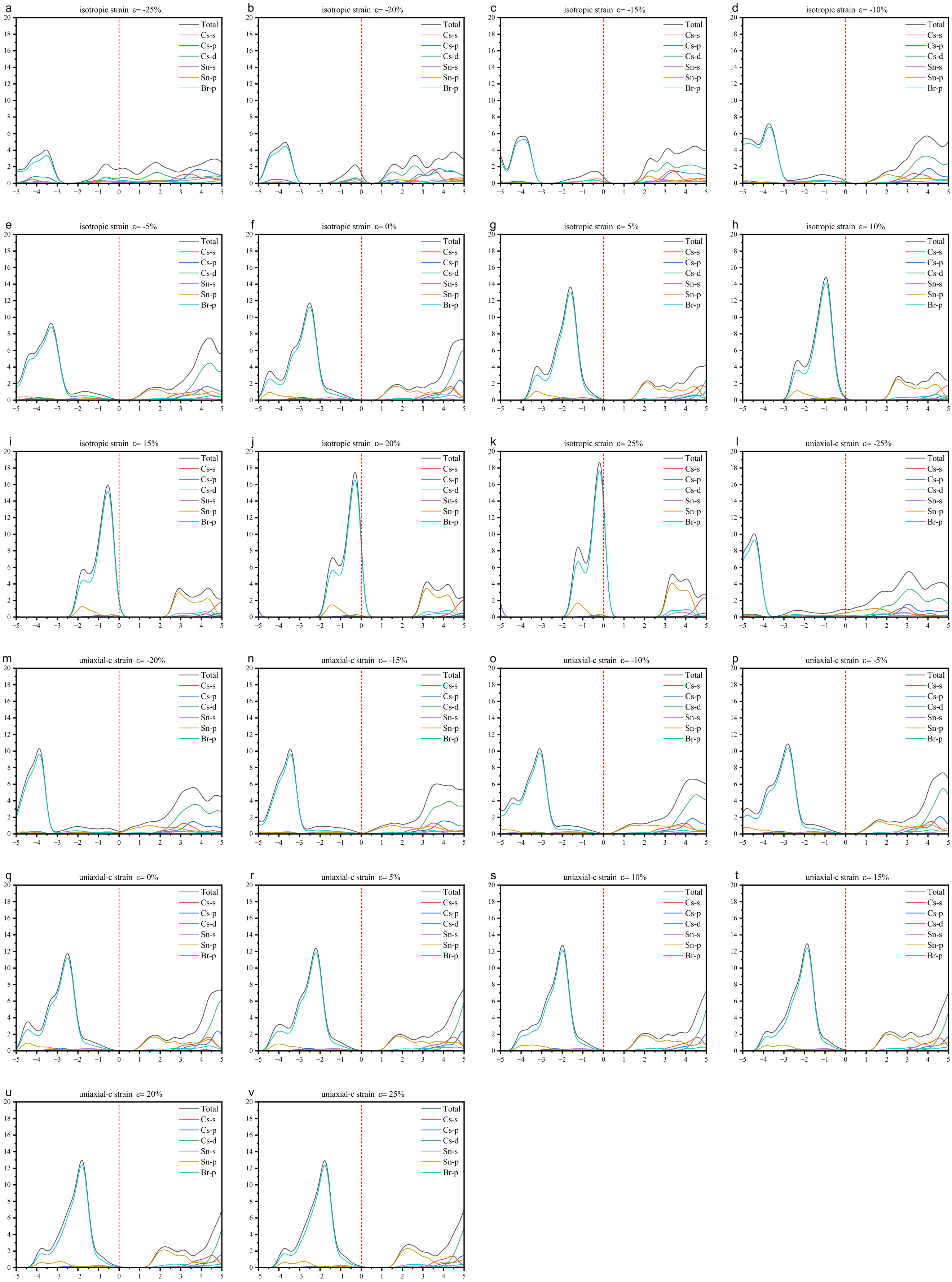


Fig. S17: $CsSnBr_3$: total and projected DOS versus strain $\varepsilon$ for isotropic and uniaxial-$c$ loading. $E_F$ is marked. States near the VBM are mainly Sn-$p$ and X-$p$; the CBM shows notable Sn-$s$ character.

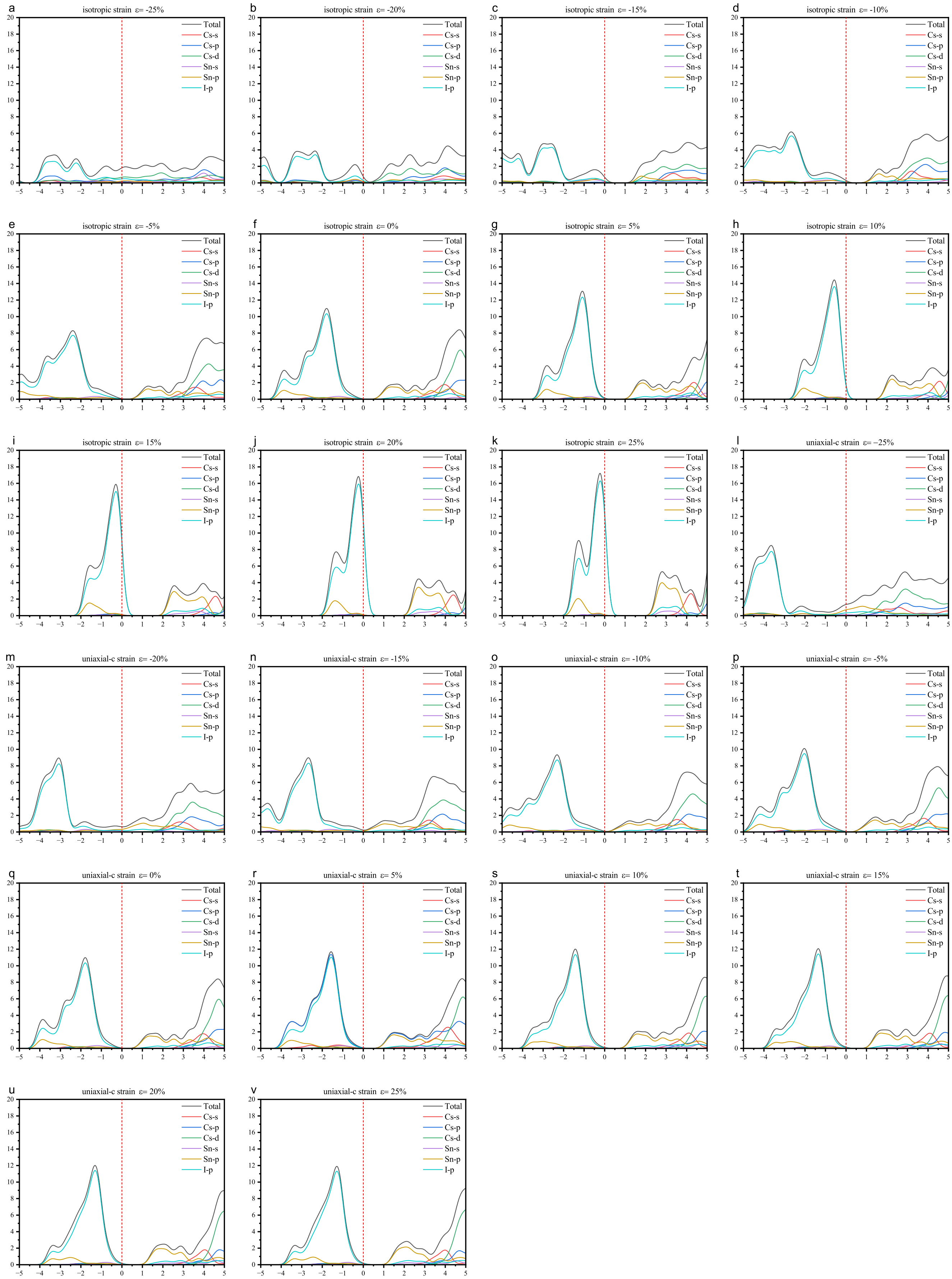


Fig. S18: $CsSnI_3$: total and projected DOS versus strain $\varepsilon$ for isotropic and uniaxial-$c$ loading. $E_F$ is marked. States near the VBM are mainly Sn-$p$ and X-$p$; the CBM shows notable Sn-$s$ character.

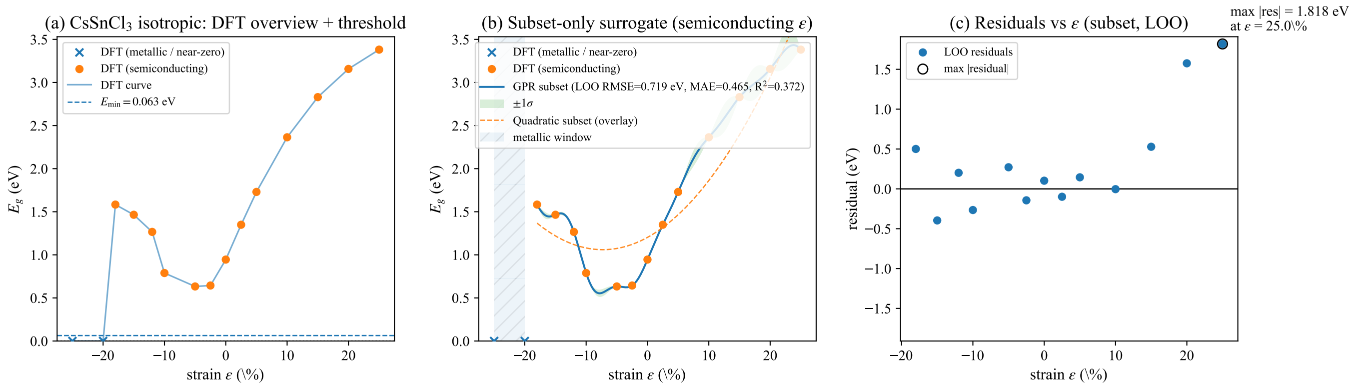


Fig. S19: $CsSnCl_3$ (isotropic): edge-case surrogate with piecewise handling. (a) DFT overview with adaptive threshold $E_{\min} = \max(0.01,\ 0.1 \times \min(E_g{>}0))$. (b) Semiconducting-subset fit (GPR RBF+white, or quadratic fallback) on $E_g > E_{\min}$ with $\pm 1\sigma$; the metallic window is shown but excluded from regression. (c) Leave-one-out residuals versus $\varepsilon$ with the largest $|r|$ highlighted.

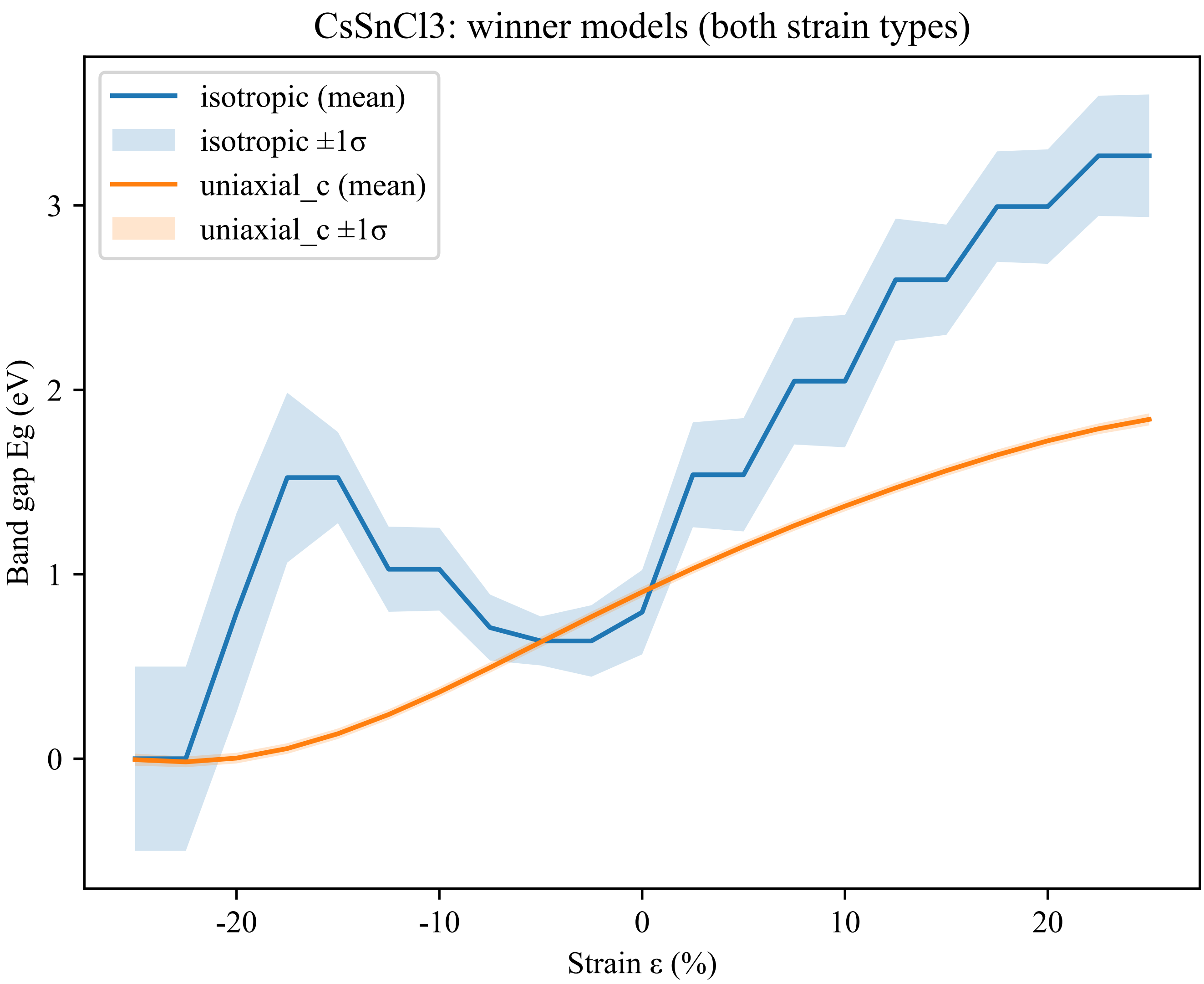


Fig. S20: $CsSnCl_3$: Winner-model predictions (mean $\pm 1\sigma$) for isotropic and uniaxial-$c$ loading. Extrapolated segments are dashed and excluded from model selection and scoring.

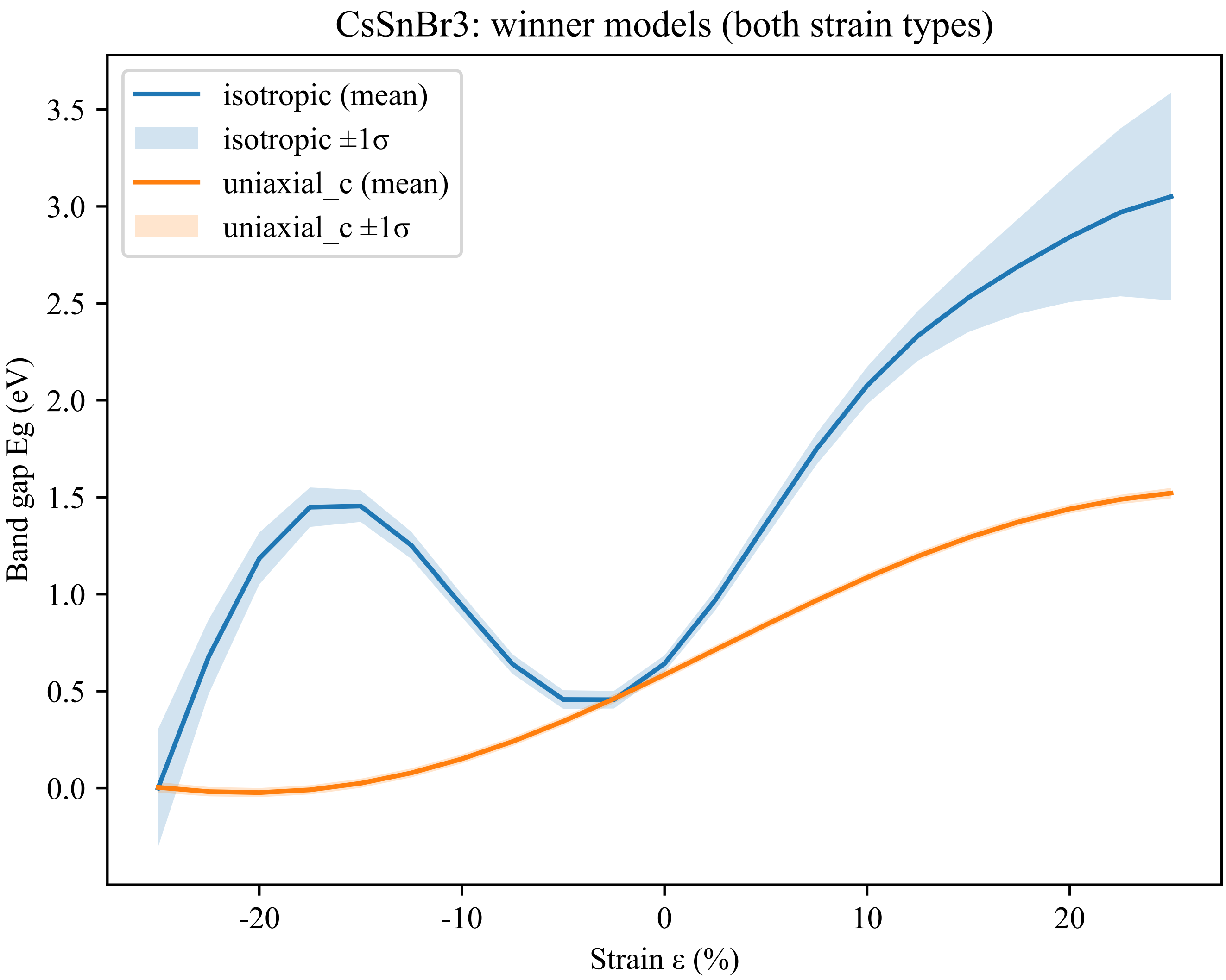


Fig. S21: $CsSnBr_3$: Winner-model predictions (mean $\pm 1\sigma$) for isotropic and uniaxial-$c$ loading. Extrapolated segments are dashed and excluded from model selection and scoring.

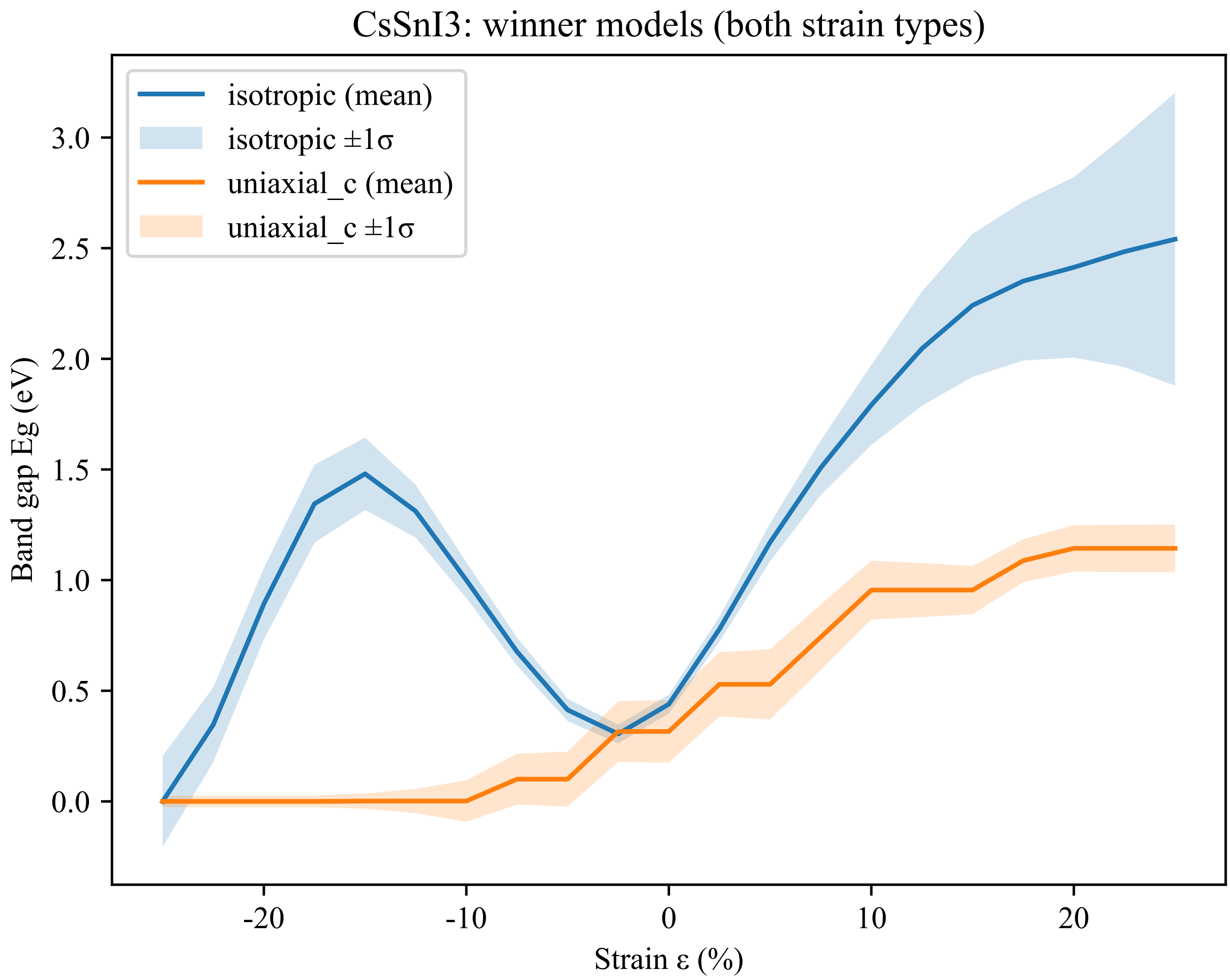


Fig. S22: $CsSnI_3$: Winner-model predictions (mean $\pm 1\sigma$) for isotropic and uniaxial-$c$ loading. Extrapolated segments are dashed and excluded from model selection and scoring.

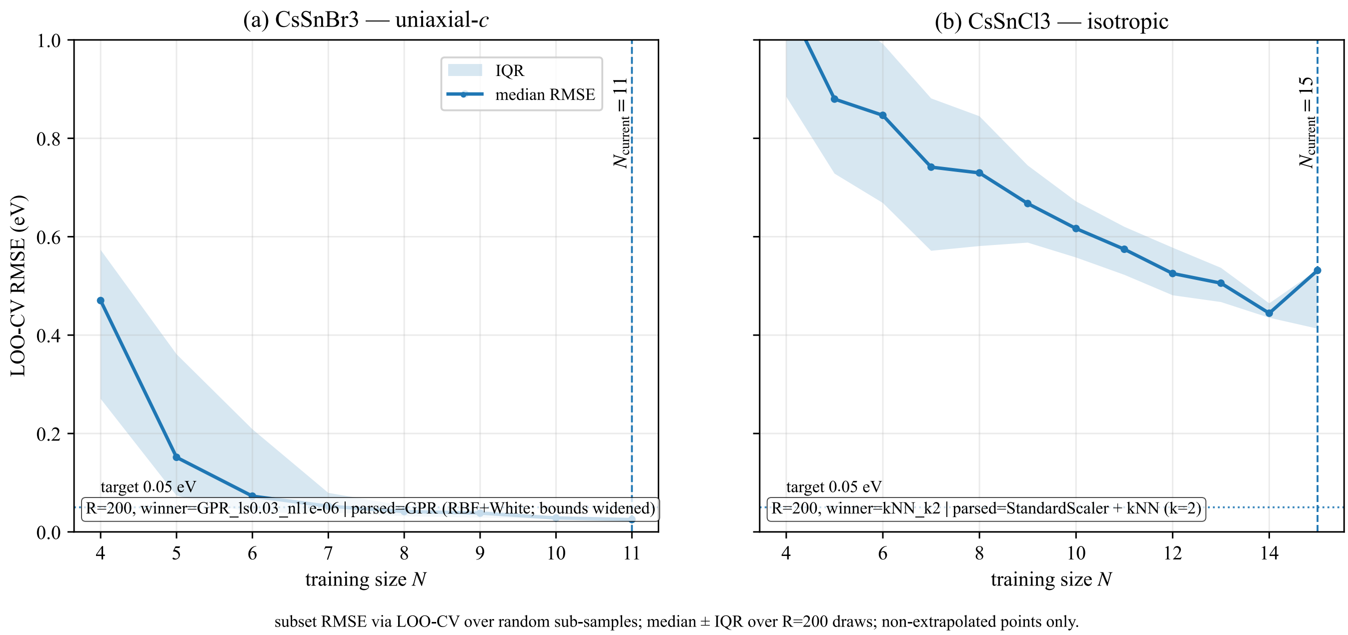


Fig. S23: $CsSnI_3$: Winner-model predictions (mean $\pm 1\sigma$) for isotropic and uniaxial-$c$ loading. Extrapolated segments are dashed and excluded from model selection and scoring.

# References

[1] A. El Badraoui, S. Dahbi, N. Tahiri, O. El Bounagui, H. Ez-Zahraouy, A DFT study of the electronic structure, optical and thermoelectric properties of perovskite CsSnBr3 compound under strains effect: Photovoltaic applications, Mod. Phys. Lett. B 38 (2024) 2350237. https://doi.org/10.1142/S0217984923502378.